Ann. Phys. (Leipzig) **13**, No. 3, 149 – 174 (2004) / **DOI** 10.1002/andp.200310069

Unconventional superconductivity and magnetism in Sr_2RuO_4 and related materials

I. Eremin[1,2,*], **D. Manske**[1], **S. G. Ovchinnikov**[3], and **J. F. Annett**[4]

[1] Institut für Theoretische Physik, Freie Universität Berlin, 14195 Berlin, Germany
[2] Physics Department, Kazan State University, 420008 Kazan, Russia
[3] L. V. Kirensky Institute of Physics, Krasnoyarsk State University, Krasnoyarsk, Russia
[4] H. H. Wills Physics Laboratory, University of Bristol, Tyndall Ave, BS8-1TL, United Kingdom

Received 1 September 2003, revised 10 December 2003, accepted 23 December 2003 by U. Eckern
Published online 16 February 2004

Key words Unconventional triplet superconductivity, spin fluctuations, strong electronic correlations
PACS 74.20.Mn, 74.70.Pq

We review the normal and superconducting state properties of the unconventional triplet superconductor Sr_2RuO_4 with an emphasis on the analysis of the magnetic susceptibility and the role played by strong electronic correlations. In particular, we show that the magnetic activity arises from the itinerant electrons in the Ru d-orbitals and a strong magnetic anisotropy occurs ($\chi^{+-} < \chi^{zz}$) due to spin-orbit coupling. The latter results mainly from different values of the g-factor for the transverse and longitudinal components of the spin susceptibility (i.e. the matrix elements differ). Most importantly, this anisotropy and the presence of incommensurate antiferromagnetic and ferromagnetic fluctuations have strong consequences for the symmetry of the superconducting order parameter. In particular, reviewing spin fluctuation-induced Cooper-pairing scenario in application to Sr_2RuO_4 we show how p-wave Cooper-pairing with line nodes between neighboring RuO_2-planes may occur. We also discuss the open issues in Sr_2RuO_4 like the influence of magnetic and non-magnetic impurities on the superconducting and normal state of Sr_2RuO_4. It is clear that the physics of triplet superconductivity in Sr_2RuO_4 is still far from being understood completely and remains to be analyzed more in more detail. It is of interest to apply the theory also to superconductivity in heavy-fermion systems exhibiting spin fluctuations.

Contents

* Corresponding author E-mail: ieremin@physik.fu-berlin.de, Phone: +49 30 838 51422, Fax: +49 30 838 57422

1 Introduction

The phenomenon of superconductivity remains one of the most interesting problems of condensed matter physics. In particular, in recent years the material science development has revealed several interesting systems where high transition temperature superconductivity was found, in particular the families of high-T_c cuprates [1] with a maximum T_c of about 155 K. Soon after their discovery it was realized that the essential physics of cuprates takes place in the CuO_2-planes which is believed to be responsible for the high transition temperature.

In this connection the discovery of superconductivity in Sr_2RuO_4 with $T_c = 1.5$ K [2] is of particular interest for several reasons. First, the crystal structure of Sr_2RuO_4 is identical to that of the parent compound of the high-T_c superconductor La_2CuO_4 (see Fig. 1 for illustration). Both kinds of materials are highly two-dimensional and as Fig. 1 shows the structure is almost identical to that of the $La_{2-x}Sr_xCuO_4$ superconductors. Both materials are oxides with conduction occurring in partially filled $d-$bands that are strongly hybridized with the oxygen p-orbitals. Therefore, it was generally believed that a comparison of the normal and superconducting properties of the cuprates and Sr_2RuO_4 will give a deeper understanding of the nature of the high-T_c in the cuprates. However, it has been found that the differences between Sr_2RuO_4 and the cuprates are larger than their general similarities might suggest. In Sr_2RuO_4 superconductivity occurs only at low temperatures and the normal state is a well-defined Fermi-liquid. This contrasts strongly with the anomalous normal state of the cuprates. Furthermore, it was soon found that the superconductivity in Sr_2RuO_4 is very interesting on its own. In particular, there are clear indications that the superconducting state is unconventional. For example, the transition temperature is highly sensitive to impurities [3] and nuclear quadrupole resonance(NQR) experiments do not show a Hebel-Slichter peak in the spin-lattice relaxation at T_c [4]. Shortly after the discovery of Sr_2RuO_4 it was suggested that superconductivity might arise from odd-parity (spin-triplet) Cooper-pairs with total spin $S = 1$ and a non-zero angular momentum which is reminiscent of the phases of superfluid ^{3}He [5]. The basis for this suggestion was the presence of ferromagnetism in the related compounds as $SrRuO_3$ and thus the expectation of ferromagnetic fluctuations in metallic Sr_2RuO_4. To support this picture the model phase diagram shown in Fig. 2 has been suggested. Here, one plots the phase of the ferromagnetic and superconducting members of the so-called Ruddlesden-Popper series ($Sr_{n+1}Ru_nO_{3n+1}$) as a function of the numbers of RuO_2-layers per unit cell, n. The infinite layer ($SrRuO_3$) is a ferromagnet with $T_{\text{Curie}} \approx 165$ K. For $n = 3$ one finds $T_{\text{Curie}} \approx 148$ K and for $n = 2$

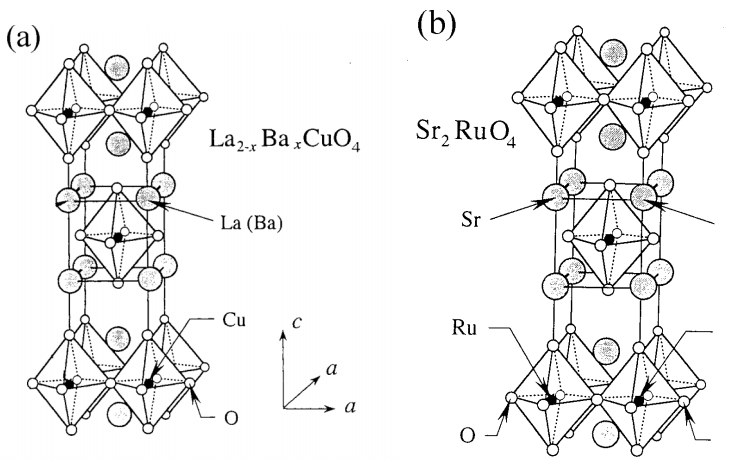

Fig. 1 Crystal structures of (a) layered cuprate singlet superconductor $La_{2-x}Sr_xCuO_4$ and (b) layered perovskite structure of the triplet superconductor Sr_2RuO_4. Both structures are identical if La (Ba) is replaced by Sr and the CuO_2-plane is replaced by RuO_2-plane.

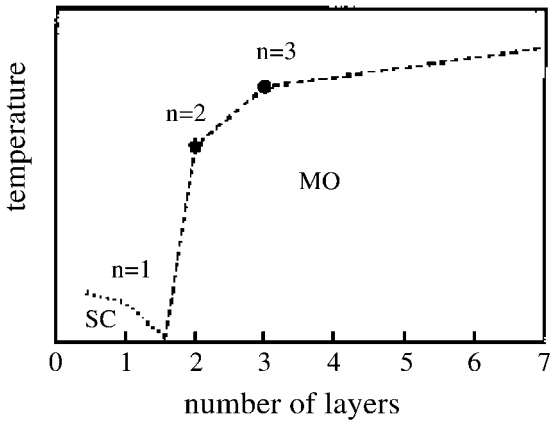

Fig. 2 Schematic phase diagram of the ferromagnetic and superconducting systems (Ruddlesden-Popper crystals) $Sr_{n+1}Ru_nO_{3n+1}$, taken from [6]. The number of layers is the parameter which determines the transition between the two phases: MO=magnetically ordered and SC=superconducting. This phase digram suggests ferromagnetic excitations in the normal state of Sr_2RuO_4.

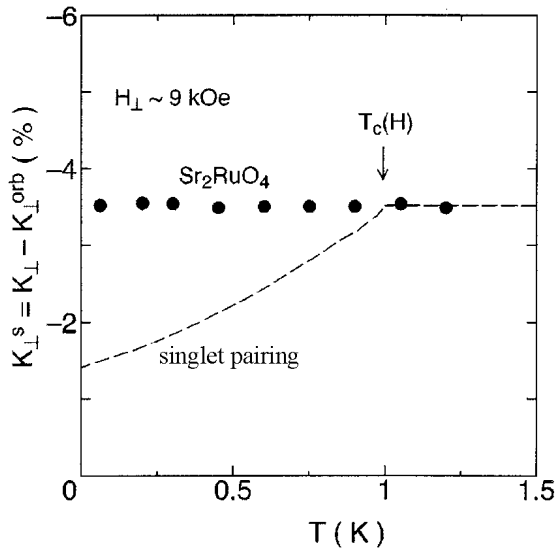

Fig. 3 Results for the uniform spin susceptibility, $\chi(\mathbf{q} = 0, \omega = 0)$ in the superconducting state of Sr_2RuO_4 as measured by NMR Knight shift [4]. One clearly sees that in contrast to the singlet Cooper-pairing (illustrated by the dashed curve) where spin susceptibility decreases upon cooling, the Knight shift in Sr_2RuO_4 is unchanged by lowering T below T_c. The Knight shift doe not decrease below T_c, since the polarization induced by the external magnetic field does not change in the superconducting state in case of spin-triplet Cooper-pairs.

the substance orders magnetically at $T_{\text{Curie}} \approx 102$ K. This demonstrates the tendency that T_{Curie} is reduced with decreasing layer number n and suggests that even for $n = 1$, when supeconductivity occurs, one expects significant ferromagnetic fluctuations which may play an important role for triplet superconductivity in Sr_2RuO_4.

Meanwhile, a number of experiments indeed point towards spin-triplet Cooper-pairing. The most convincing evidence comes from the ^{17}O NMR Knight shift data which shows that the spin susceptibility is not affected by the superconducting state for a magnetic field parallel to the RuO_2-plane [4]. In Fig. 3 we show the corresponding experimental results. In conventional superconductors the spin part of the Knight shift measured by NMR decreases rapidly below T_c due to the formation of singlet Cooper-pairs. On the other hand, in a triplet superconductor with S=1 the spin part of the Knight shift should not change below T_c for some field orientations, since the polarization induced by the weak external magnetic field and probed by NMR does not change. This behavior was observed in Sr_2RuO_4 by Ishida et al. [4] and provides strong evidence for triplet Cooper-pairing.

However, recently it has became clear that the situation is not that simple. For example, the intensive studies by means of inelastic neutron scattering (INS) reveal the presence of strong two-dimensional antiferromagnetic spin fluctuations at $\mathbf{Q} = (2\pi/3, 2\pi/3)$ and no sign of ferromagnetic fluctuations in the normal state of Sr_2RuO_4 [7]. This fact, at first glance, cannot be compatible with triplet Cooper-pairing and thus the role of the antiferromagnetic fluctuations in the formation of superconductivity has to be clarified.

Moreover, further analysis of the NMR data indicated the magnetic response to be strongly anisotropic [8]. In particular, the measured longitudinal component of the spin susceptibility χ_{zz} is much larger than the transverse one χ_{+-}, while from an isotropic model one expects $\chi_{+-} = 2\chi_{zz}$. This anisotropy increases with decreasing temperature and reaches a maximum close to T_c indicating its influence on the superconducting properties. Therefore, in view of the importance of spin fluctuations for the unconventional superconductivity in Sr_2RuO_4 their behavior should be understood in more detail.

Another interesting question concerns the symmetry of the superconducting order parameter. While the analogy to the case of superfluid ^{3}He leads to the suggestion of nodeless p-wave superconductivity in Sr_2RuO_4, recent analysis of the specific heat data [9] indicates a more complicated and anisotropic behavior of the superconducting order parameter in the first Brillouin Zone (BZ). Therefore, the physics of Sr_2RuO_4 is far from being completely understood.

Note, an extensive review on the experimental situation can be found in [10]. In contrast to that review, in the present review we mainly analyze the role played by strong electronic correlations and spin fluctuations in Sr_2RuO_4. So far their role in determining the superconducting and normal state properties has not been addressed in detail. Probably, this was due to the success of the conventional band theory in explaining the various properties of Sr_2RuO_4. However, its success is mainly due to the correct description of the Fermi surface topology in this compound. The Fermi surface shape, however, is hardly affected by the electronic correlations, while on the other hand the bandwidth and the energy dispersion are strongly modified. We will show that this is indeed the case for the ruthenates. Furthermore, we review the spin-fluctuation mediated Cooper-pairing scenario in application to Sr_2RuO_4 and address the important role of spin-orbit coupling in this system. In particular, we discuss the symmetry of the relevant superconducting order parameter within this scenario and, finally, investigate the role of impurities in Sr_2RuO_4.

2 Superconductivity and magnetism in Sr_2RuO_4

2.1 Electronic structure and Fermi surface

In Sr_2RuO_4 the formal valence of the ruthenium ion is Ru^{4+}. This leaves four electrons remaining in the $4d$-shell. Furthermore, the Ru ion sits at the center of a RuO_6-octahedron and the crystal field of the O^{2-} ions splits the five $4d$-states into threefold (t_{2g}) and twofold (e_g) subshells as illustrated in Fig. 4. The negative charge of the O^{2-} ions causes the t_{2g} subshell to lie lower in energy. Note, that these orbitals (xz, yz, and xy) have lobes that point between the O^{2-} ions lying along the x, y, and z-axes. Electrons of these orbitals form the Fermi surface (the so-called α, β, and γ-bands). We assume that the most important interaction of the carriers is with spin excitations described by the spin susceptibility $\chi(\mathbf{q}, \omega)$ and resulting from Ru α-, β-, and γ-states. Then, we have 3 bands formed out of the oxygen $p-d$-π hybridized orbitals and with a filling factor of 4/3. Since $p-d$-π bonding is weaker than the $p-d$-σ realized in cuprates, the admixture of the oxygen orbitals is smaller in ruthenates than in cuprates. For example, the contribution of the oxygen p-states close to the Fermi level is only 16 percent in Sr_2RuO_4. At the same time the contribution of the

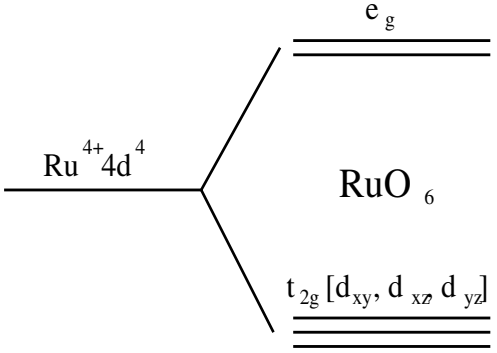

Fig. 4 Electronic structure of Sr_2RuO_4. The Ru^{4+} ion corresponds to a $4d^4$ level. The splitting of the e_g and t_{2g} subshells is due to the RuO_6 crystal field. The orbitals d_{xy}, d_{xz}, and d_{yz} cross the Fermi level and form the α-, β-, and γ-band. The resulting band structure is quasi-two-dimensional. Magnetic activity results from the t_{2g} subshell.

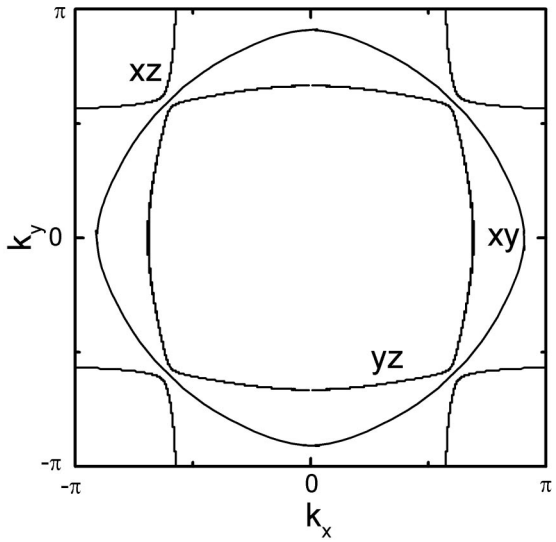

Fig. 5 Calculated two-dimensional Fermi surface of Sr_2RuO_4 using eq. (1). The Fermi surface consists of three sheets: two with electron-like topology and one with hole-like topology. Note, the quasi-one-dimensional character of the α(xz)- and β(yz)-bands.

Ru $4d$-orbitals is about 84 percent [11]. LDA calculations [12, 13] indeed confirm the existence of the three bands crossing the Fermi level.

The band structure of Sr_2RuO_4 is quasi-two-dimensional and the electronic dispersion along the c-axis is very small [13]. This is because the highly planar structure of Sr_2RuO_4 prevents substantial energy dispersion along the z-direction, due to the large interplanar separation of the RuO_6 octahedra. At the same time, in the ab-plane neighboring RuO_6-octahedra share O ions which in turn are π-bonded to the Ru ions. Thus, the xy-orbital will form a two-dimensional band, while the xz- and yz-bands have only a restricted one-dimensional character. Then, to describe the LDA results the following tight-binding energy dispersions can be introduced

$$\epsilon_{\mathbf{k}} = -\epsilon_0 - 2t_x \cos k_x - 2t_y \cos k_y + 4t' \cos k_x \cos k_y \,. \tag{1}$$

The lattice constants $a = b$ have been set to unity. This model is a good parameterization of LDA calculations [14] if one chooses for d_{xy}-, d_{zx}-, and d_{yz}-orbitals the values for the parameter set $(\epsilon_0, t_x, t_y, t')$ as (0.5, 0.42, 0.44, 0.14), (0.23, 0.31, 0.045, 0.01), and (0.23, 0.045, 0.31, 0.01) eV. The experimental investigation of the Fermi surface made by means of de-Haas-van-Alphen effect completely confirmed the LDA results [15]. The resulting Fermi surface is shown in Fig. 5. Here, the α-band is hole-like centered around (π, π) point of the Brillouin Zone, while β and γ-bands are electron-like ones centered around Γ-point. Furthermore, as one sees the α and β-bands are quasi-one-dimensional and their degeneracy is removed by the introduction of the interband (between α and β-bands) hopping $t_\perp = 0.025\,\mathrm{eV}$ [13].

Despite of the large difference in the magnitudes of the resistivity in the RuO_2-plane and perpendicular to the planes, $\rho_c/\rho_{ab} \geq 500$, the temperature dependences of ρ_c and ρ_{ab} for $T < 25$ K both follow the Fermi-liquid behavior $\propto T^2$ [3]. Above $T = 25$ K small deviations from this law occur. At higher temperatures ρ_{ab} becomes linear with a temperature dependence similar to the cuprates.

2.2 Dynamical spin susceptibility and electronic correlations

As already mentioned in the introduction, the spin dynamics of Sr_2RuO_4 consists of ferromagnetic and incommensurate antiferromagnetic spin fluctuations at wave vector $\mathbf{Q}_i = (2\pi/3, 2\pi/3)$. Its role in the formation of triplet superconductivity in Sr_2RuO_4 requires special consideration.

Long-range magnetic order is absent in Sr_2RuO_4. On the other hand the uniform magnetic susceptibility is much larger than the Pauli susceptibility of the non-interacting electrons. Indeed the 'ab-initio' calculations of the Stoner factor $IN(0)$ (where I is the exchange parameter at $\mathbf{q} = 0$, $N(0)$ is the density of states at

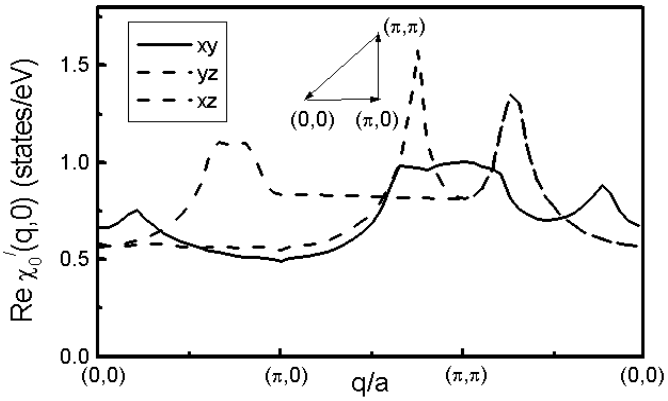

Fig. 6 Calculated real part of the Lindhard spin susceptibility χ_0^l (l refers to the band indices) in the normal state of Sr_2RuO_4 along the route $(0,0) \rightarrow (\pi,0) \rightarrow (\pi,\pi) \rightarrow (0,0)$ in the first BZ for the three different orbitals (xz,yz, and xy) crossing the Fermi level. Due to the nesting of the xz and yz-bands their susceptibilities show an enhancement at the incommensurate antiferromagnetic wave vector $\mathbf{Q}_i = (2\pi/3, 2\pi/3)$. The response of the xy-band is more isotropic, but significantly larger than in the normal metal due to the vicinity of the Van-Hove singularity.

the Fermi level) gives the following values $IN(0) = 0.82$ [12], $IN(0) = 0.89$ [13]. Using a simple so-called Stoner criterium, this indicates that Sr_2RuO_4 is in the vicinity of the instability to ferromagnetism. In $SrRuO_3$ the corresponding Stoner parameter is $IN(0) = 1.23$ [16]. Therefore, this system is a ferromagnetic metal with magnetic moment $1.6\mu_B$ and Curie temperature $T_c = 150$ K. The reason for the enhanced ferromagnetic exchange fluctuations in $SrRuO_3$ in comparison to Sr_2RuO_4 is the stronger $p-d$ hybridization and thus a larger contribution of the oxygen p-orbitals in the density of states at the Fermi level.

However, what is interesting in Sr_2RuO_4 is not only the presence of ferromagnetic fluctuations at $\mathbf{q} = 0$ (from the Stoner instability), but also the incommensurate antiferromagnetic fluctuations at the wave vector $\mathbf{Q}_i = (2\pi/3, 2\pi/3)$ as observed in inelastic neutron scattering experiments [7]. What is the origin of these fluctuations? In fact they originate from the nesting properties of the quasi-one-dimensional xz- and yz-bands. In order to see this we show in Fig. 6 the results for the Lindhard response functions calculated for the different bands using their tight-binding dispersions

$$\chi_0^i(\mathbf{q},\omega) = -\frac{1}{N}\sum_{\mathbf{k}} \frac{f^i_{\mathbf{k}} - f^i_{\mathbf{k}+\mathbf{q}}}{\epsilon^i_{\mathbf{k}} - \epsilon^i_{\mathbf{k}+\mathbf{q}} + \omega + i0^+}\,, \tag{2}$$

where i refers to the band index and $f_{\mathbf{k}}$ is the Fermi distribution function. As seen in Fig. 6, due to the pronounced nesting of the xz and yz-bands their susceptibilities display peaks at $\mathbf{Q}_i = (2\pi/3, 2\pi/3)$, while the xy-band does not show any significant feature. The response of the xy-band is enhanced due to the presence of the van-Hove singularity close to the Fermi level. Then, it becomes clear that the features observed by INS relate mainly to the magnetic response of the xz- and yz-bands. Furthermore, as has been shown in [17] that the Stoner enhancement related to the appearance of the incommensurate antiferromagnetic fluctuations is even stronger than the ferromagnetic one and is of the order of 1. This means that Sr_2RuO_4 is almost unstable with respect to the spin density wave formation (SDW). Note, that both ferromagnetic and antiferromagnetic fluctuations are seen experimentally in the normal state of Sr_2RuO_4 by means of ^{17}O Knight shift [18] and by inelastic neutron scattering [7], respectively.

These results suggest that an effective Hamiltonian for describing the physics in Sr_2RuO_4 is a two-dimensional three-band Hubbard Hamiltonian

$$H = \sum_{\mathbf{k},\sigma}\sum_{\alpha} \epsilon_{\mathbf{k}\alpha} a^+_{\mathbf{k},\alpha\sigma} a_{\mathbf{k},\alpha\sigma} + \sum_{i,\alpha} U_\alpha\, n_{i\alpha\uparrow} n_{i\alpha\downarrow}\,, \tag{3}$$

where $a_{\mathbf{k},\alpha\sigma}$ is the Fourier transform of the annihilation operator for the d_α orbital electrons ($\alpha = xy, yz, zx$) and U_α is an effective on-site Coulomb repulsion. The hopping integrals $t_{\mathbf{k}\alpha}$ denote the energy dispersions of the tight-binding bands, see eq. (1).

As a result the spin dynamics in Sr_2RuO_4 is determined by the competition and the delicate balance between ferromagnetic and incommensurate antiferromagnetic fluctuations. The natural question arises

what is the influence of these magnetic fluctuations on the triplet superconductivity in Sr_2RuO_4? In the following subsection we will study the formation of triplet of superconductivity in Sr_2RuO_4 driven by the spin fluctuation exchange.

In the remainder of this section we discuss another aspect of the ruthenates, namely strong electronic correlations. As a matter of fact the success of 'ab-initio' methods in describing magnetism of Sr_2RuO_4 appear to invalidate, at first sight, the discussion of the role of strong electronic correlations. On the other hand, the effects of strong electronic correlations are small if the bandwidth of the conduction band W is much larger than the on-site Coulomb repulsion, U. Given that the bandwidth is of the order of 1 eV there is no reason to think that $W >> U$ in Sr_2RuO_4. To estimate the value of U one has to remember that for $4d$-electrons U has to be smaller than for $3d$-electrons, since the average radius of the $4d$-shell is approximately two times larger than for the $3d$-shell. Then a simple estimates gives $U_{Ru} \approx 1$ eV. This means that Sr_2RuO_4 is in the regime of intermediate electronic correlations when $U \sim W$.

As we mentioned earlier, despite of the importance of the electronic correlations in Sr_2RuO_4 the relative success of the band structure theory can be easily explained. The correct description of the ferromagnetic and antiferromagnetic fluctuations comes from the correct Fermi surface topology which is not affected by the electronic correlations. However, the bandwidth and the energy dispersion are strongly affected by the electronic correlations in Sr_2RuO_4. For example, it has been shown by Liebsch and Lichtenstein [14] that in order to explain the bandwidth as measured by angle-resolved photoemission spectroscopy (ARPES) the electronic correlations have to be taken into account. In particular, using dynamical-mean-field theory (DMFT) they have shown that, while the Fermi surface topology is the same independent on electronic correlations, the bandwidth is different, namely the correlations reduce the bandwidth of the all bands in Sr_2RuO_4. We will further address this issue discussion the phase diagram of $Ca_{2-x}Sr_xRuO_4$.

2.3 Superconducting state of Sr_2RuO_4: role of spin fluctuations and symmetry of the superconducting order parameter

Even before experimental results have indicated triplet superconductivity in Sr_2RuO_4, its possibility had been theoretically predicted by Sigrist and Rice [5]. In particular, they considered the triplet superconductivity on a square lattice as an electronic analogy of the superfluid A-phase in ^{3}He.

For the spin-triplet Cooper-pairing the wave function can be written as a matrix in spin space

$$\Psi = g_1(k)|\uparrow\uparrow> + g_2(k)\,(|\uparrow\downarrow> + |\downarrow\uparrow>) + g_3(k)|\downarrow\downarrow> = \begin{pmatrix} g_1(k) & g_2(k) \\ g_2(k) & g_3(k) \end{pmatrix}, \tag{4}$$

where the eigenvalues of the S_z operator with projection +1, 0, -1 have the form

$$|\uparrow\uparrow> = \begin{pmatrix} 1 & 0 \\ 0 & 0 \end{pmatrix}, \qquad |\uparrow\downarrow> + |\downarrow\uparrow> = \begin{pmatrix} 0 & 1 \\ 1 & 0 \end{pmatrix}, \qquad |\downarrow\downarrow> = \begin{pmatrix} 0 & 0 \\ 0 & 1 \end{pmatrix}. \tag{5}$$

Another possibility to express the Cooper-pair wave function is to use the basis of the symmetric matrices

$$i\sigma\sigma_y = (i\sigma_x\sigma_y, i\sigma_y\sigma_y, i\sigma_z\sigma_y). \tag{6}$$

Then the Cooper-pair wave function has the form

$$\Psi = i\,(\mathbf{d}(\mathbf{k})\cdot\sigma) = \begin{pmatrix} -d_x + id_y & d_z \\ d_z & d_x + id_y \end{pmatrix}. \tag{7}$$

The components of the vector $\mathbf{d}$ can be expressed linearly via the amplitudes of $g_\alpha(\mathbf{k})$:

$$g_1 = -d_x + id_y\,, \qquad g_2 = d_z\,, \qquad g_3 = d_x + id_y\,. \tag{8}$$

Due to the Pauli principle the orbital part of the wave function with total $S = 1$ has to be odd, i.e. the orbital quantum number $l = 1, 3, \ldots$. Therefore, one can speak about p, f, ... Cooper-pairing in a continuum system. In particular, the amplitudes $g_\alpha(\mathbf{k})$ and the vector $\mathbf{d}(\mathbf{k})$ have to be the odd functions of the momentum $\mathbf{k}$.

In the tetragonal crystal structure such as that of Sr_2RuO_4, the order parameter $\mathbf{d}(\mathbf{k})$ has to belong to the corresponding irreducible representation of the D_{4h} group. There are several representations [5, 19] and the proper choice can be made by comparison to experiment. For example, the spin state of the Cooper-pair wave function can be obtained from the measuring the Knight shift in NMR and polarized inelastic neutron scattering experiments below T_c. The orbital state can be measured by muon spin relaxation (μSR) indicating time-reversal symmetry breaking. The square symmetry of the vortex lattice can also be interpreted as evidence for p-wave pairing.

As we have shown in the introduction, the NMR Knight shift experiments indicate spin-triplet Cooper-pairing in Sr_2RuO_4 [4]. The same conclusion has been drawn from the polarized neutron scattering studies [20]. The time-reversal symmetry breaking detected by means of the μSR [21] suggests the superconducting order parameter E_u with $S_z = 0$ and $l_z = \pm 1$ (so-called chiral p-wave state):

$$d_z = \hat{\mathbf{z}}\Delta_0(\sin k_x \pm i \sin k_y)\,, \qquad \hat{\mathbf{z}} = |S_z = 0> \,. \tag{9}$$

The amplitude of this gap is isotropic, $\Delta_{\mathbf{k}} = \Delta_0\sqrt{k_x^2 + k_y^2}$, and does not have a node at the Fermi surface of Sr_2RuO_4.

So far, the above analysis is quite general. Next, we assume the superconductivity is driven by the exchange of spin fluctuations. The interesting question in the ruthenates is why does triplet Cooper-pairing take place in the presence of strong incommensurate antiferromagnetic spin fluctuations at $\mathbf{Q}_i = (2\pi/3, 2\pi/3)$ originating from the xz- and yz-bands and only relatively weak ferromagnetic fluctuations arising from the xy-band. In general, to answer this question the BCS gap equation (see eq. (16)) must be solved assuming different possible symmetries of the order parameter and corresponding pairing interaction for singlet, triplet with $S_z = 0$ projection and triplet with $S_z = \pm 1$ projection Cooper-pairing. For the analysis of the interaction between quasiparticles and spin fluctuations (ferromagnetic and incommensurate antiferromagnetic) we use the generalized Eliashberg like theory for the interaction between quasiparticles and spin fluctuations [22]. We extend this theory to become a three-band theory, as necessary in Sr_2RuO_4 [23, 24].

In the normal state both the self-energy and thermal Green's functions become matrices of 3×3 form, i.e. $G_{i,j,m}(\mathbf{k}, \omega_n)$ and $\Sigma_{i,j,m}(\mathbf{k}, \omega_n)$, where i, j, m refer to the band indexes of the xy, yz, and xz-orbitals. The corresponding Dyson equation is given by

$$\left[\hat{G}(\mathbf{k}, \omega_n)\right]^{-1} = \left[\hat{G}^0(\mathbf{k}, \omega_n)\right]^{-1} - \hat{\Sigma}(\mathbf{k}, \omega_n), \tag{10}$$

where $\hat{G}^0_{i,j,m}(\mathbf{k}, \omega_n)$ is the matrix of the bare Green's function determined via the tight-binding energy dispersions for the xy, yz, and xz-bands. The self-energy is given by

$$\Sigma_{i,j,m}(\mathbf{k}, \omega_n) = T\sum_{q,l} V^1_{i,j,m}(\mathbf{q}, \omega_l) \times G_{i,j,m}(\mathbf{k} - \mathbf{q}, \omega_n - \omega_l)\,, \tag{11}$$

where $V^1_{i,j,m}(\mathbf{q}, \omega_l)$ is an effective interaction between quasiparticles and spin fluctuations. As shown in Fig. 7 it consists of an infinite series of diagrams including charge and spin fluctuations. This is similar to the case of cuprates, however, some important differences are present in the random phase approximation.

Most importantly we must now consider the diagrams shown in Fig. 8 with an odd number of bubbles that contribute to the triplet pairing. This is in contrast to singlet pairing in cuprates where an even number of bubbles occur (see Fig. 7). Furthermore, the transverse (+-) and the longitudinal (zz) parts of the spin susceptibility are different. The reason for this (as we show later) is the presence of spin-orbit coupling. We

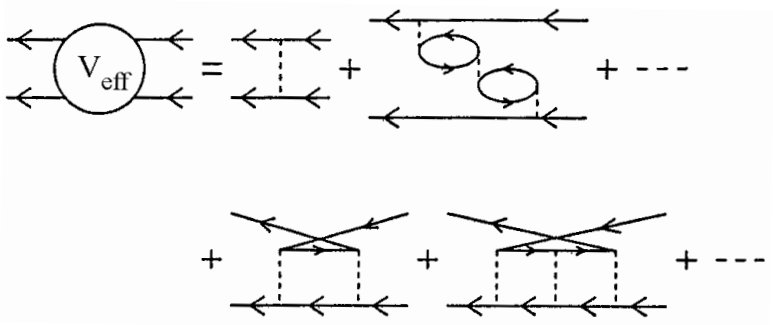

Fig. 7 Lowest order RPA diagrams for the effective pairing interaction $V_{\rm eff}$ for singlet pairing resulting from the exchange of longitudinal and transverse spin and charge fluctuations. The solid lines refer to the one-particle Green's function and the dashed lines denote an effective Coulomb interaction U. The first diagram leads to a renormalized chemical potential. Note that for singlet pairing only an even number of bubble diagrams occur due to Pauli's principle.

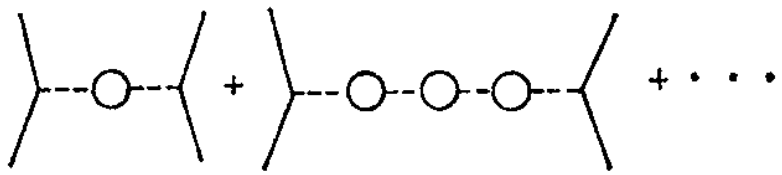

Fig. 8 Additional RPA diagrams of the lowest order for triplet Cooper-pairing with odd number of bubbles that refer to longitudinal charge and spin fluctuations.

discuss its role in detail in the next section. Then the effective pairing interaction in the 3×3 form including transverse and longitudinal spin fluctuations and also charge fluctuations is given by

$$V^{1}_{i,j,m}(\mathbf{q},\omega_l) = \tfrac{1}{2} V^{{\rm sp},zz}_{i,j,m}(\mathbf{q},\omega_l) + V^{{\rm sp},+-}_{i,j,m}(\mathbf{q},\omega_l) + \tfrac{1}{2} V^{\rm ch}_{i,j,m}(\mathbf{q},\omega_l)\,, \tag{12}$$

where

$$V^{{\rm sp},zz} = U^2 \frac{\chi_0^{{\rm sp},zz}}{1 - U\chi_0^{{\rm sp},zz}}\,, \qquad V^{{\rm sp},+-} = U^2 \frac{\chi_0^{{\rm sp},+-}}{1 - U\chi_0^{{\rm sp},+-}} \tag{13}$$

describe coupling to spin density fluctuations and

$$V^{\rm ch} = U^2 \frac{\chi_0^{\rm ch}}{1 + U\chi_0^{\rm ch}} \tag{14}$$

to charge density fluctuations. $\chi_0^{\rm ch}$, $\chi_0^{{\rm sp},+-}$ are the irreducible parts of the charge and spin susceptibilities respectively. Note that in the Bethe-Salpether equation shown diagrammatically in Fig. 7 for singlet Cooper-pairing it is necessary to have an even number of bubbles and include the ladder diagrams. In the case of triplet Cooper-pairing the contribution of the ladder diagrams is zero and an odd number bubbles diagrams

occur due to Pauli's principle shown in Fig. 8. Since the Feynman rules require a (-1) for each loop an extra minus sign enters the gap equation via $V_t^{\rm eff}$.

The magnetism in the ruthenates resulting from the quasiparticles in the t_{2g}-orbital is itinerant and thus the magnetic response is created by the same electrons that form also the Cooper-pairs. Then, for example, the irreducible part of the charge susceptibility $\chi_0^{\rm ch}$ is defined in terms of the electronic Green's functions

$$\chi_0^{\rm ch}(\mathbf{q}) = \frac{1}{N}\sum_{\mathbf{k}} G(\mathbf{k}+\mathbf{q})G(\mathbf{k}), \tag{15}$$

where $G(\mathbf{k})$ is the single-electron Green's function (we omit here the band indices for simplicity). The longitudinal and transverse components of the spin susceptibilities are also calculated in terms of the electronic Green's functions. In contrast to the cuprates, in the ruthenates $\chi_0^{\rm sp,zz}$ and $\chi_0^{\rm sp,+-}$ are different due to the magnetic anisotropy [4].

In the ruthenates the general matrix form of the superconducting gap equation for $\Delta(\mathbf{k},\omega)$ is similar to the case of cuprates. To determine the superconducting transition temperature T_c one must solve the following set of linearized gap equations to obtain $\lambda_\mu(T)$:

$$\lambda_\mu \Delta_{\mu,l,m}(\mathbf{k},\omega_n) = -\frac{T}{N}\sum_{k',\omega_j}\sum_{l',m'} V^{(2)}_{\mu,l,m}(\mathbf{k}-\mathbf{k}',\omega_n-\omega_j)\, G_{ll'}(\mathbf{k}',\omega_j) \times G_{mm'}(-\mathbf{k}',-\omega_j)\, \Delta_{\mu,l',m'}(\mathbf{k}',\omega_j). \tag{16}$$

Here, λ_μ is an eigenvalue and T_c is determined from the condition $\lambda(T_c)=1$.

Note, the interband coupling will provide a single T_c for all three bands. The pairing potential $V^{(2)}$ (taken for singlet or triplet pairing) controls which state gives the lowest energy and determines singlet or triplet Cooper-pairing. Three possibilities may occur:

(a) singlet pairing,
(b) triplet pairing with the total spin $S_z = 0$ of the Cooper-pair wave function,
(c) triplet pairing with the total spin $S_z = \pm 1$.

Note, a priori one cannot judge which pairing state is realized in the ruthenates due to the presence of both antiferromagnetic and ferromagnetic fluctuations. Therefore, one has to solve the gap equations for all three possibilities. Thus, for singlet pairing we use

$$V_s^{(2)} = \tfrac{1}{2}V_{\rm sp}^{zz} + V_{\rm sp}^{+-} - \tfrac{1}{2}V_{\rm ch}\,. \tag{17}$$

For triplet pairing with $S_z = \pm 1$ we take

$$V_{\rm tr1}^{(2)} = -\tfrac{1}{2}V_{\rm sp}^{zz} - \tfrac{1}{2}V_{\rm ch} \tag{18}$$

resulting from the set of diagrams with odd number of bubbles (see Fig. 8). Finally, for triplet pairing with $S_z = 0$ we get

$$V_{\rm tr0}^{(2)} = \tfrac{1}{2}V_{\rm sp}^{zz} - V_{\rm sp}^{+-} - \tfrac{1}{2}V_{\rm ch}\,. \tag{19}$$

Therefore due to magnetic anisotropy we have separated the longitudinal and transverse parts of the spin fluctuations. Note, transverse and longitudinal spin fluctuations contribute differently to the singlet and triplet Cooper-pairing. In particular, in the spin-triplet case the longitudinal and transverse spin fluctuations do not act additively as in the case of singlet Cooper-pairing. As a result, a strong reduction of the superconducting transition temperature T_c is expected. The effect of charge fluctuations is expected to be small in the superconductivity in Sr_2RuO_4.

The pairing state symmetry is determined at T_c by the eigenvector of eq. (16) corresponding to $\lambda_\mu(T) = 1$. As well as in the case of superfluid ^{3}He many other possible states besides the A-phase can occur. Note, that recent experiments indicate the occurrence of the line nodes in the superconducting state of Sr_2RuO_4. These are the power rather an exponential laws of the specific heat, $C(T) \propto T^2$ [25], spin-lattice relaxation rate $1/T_1 \propto T^3$ [26], the heat capacity $\kappa \propto T^2$ [27], and ultrasound attenuation [28]. Therefore, other symmetries of the superconducting order parameter like p-wave symmetry with nodes or f-wave symmetry which are other than simple nodeless p-wave symmetry of the superconducting gap have to be considered. Note, the largest eigenvalue of eq. (16) corresponds to a minimum in the free energy and thus will yield the symmetry of the superconducting order parameter Δ_l in Sr_2RuO_4. One could expect that the formation of the node should correspond to the influence of the incommensurate antiferromagnetic fluctuations. Let us see whether the simple nodeless p-wave symmetry is possible if the IAF at the wave vector $\mathbf{Q} = (2\pi/3, 2\pi/3)$ are present.

Using appropriate symmetry representations [5] we discuss the solutions of the gap equation assuming p, d, or f-wave symmetry of the order parameter in the RuO_2-plane [29]:

$$\mathbf{d}_p(\mathbf{k}) = \Delta_0 \hat{\mathbf{z}}(\sin k_x a + i \sin k_y a), \tag{20}$$

$$\Delta_d(\mathbf{k}) = \Delta_0(\cos k_x a - \cos k_y a), \tag{21}$$

$$\mathbf{d}_{f_{x^2-y^2}}(\mathbf{k}) = \Delta_0 \hat{\mathbf{z}}(\cos k_x a - \cos k_y a)(\sin k_x a + i \sin k_y a). \tag{22}$$

Here the $\hat{\mathbf{z}}$-unit vector refers to the d_z component of the Cooper-pairs as observed in the experiment [32]. We will present a possible explanation for this below. These symmetries of the superconducting order parameter must be substituted into the eq. (16). For simplicity we consider first the solution of eq. (16) in the RuO_2-planes and then discuss what is happening along the c-axis.

Solving eq. (16) in the first BZ down to 5 K we have found that p-wave symmetry yields the largest energy gain for the $xy-$band, while for the $xz-$ and $yz-$bands the situation is more complicated. We find that the gap equations for the xy- and $yz-$, xz-bands can be separated due to their weak interaction. The result is that for the xy-band the p-wave is the most stable solution, while for the $xz-$ and $yz-$bands $f_{x^2-y^2}$-wave symmetry yields the largest eigenvalue due to stronger nesting.

How to understand the competition between p- and f-wave pairing? For doing this we display in Fig. 9 characterizes the solutions of eq. (16). Note, a good approximation is to linearize eq. (16) with respect to Δ_l^i, i.e. $E_{\mathbf{k}'}^i \to \epsilon_{\mathbf{k}'}^i$. We use also $\tanh(\epsilon_{\mathbf{k}'}^i/2k_BT) = 1$. Thus, the main contribution to the pairing comes from the states at the Fermi level. We present our results in terms of the Fermi surface of the RuO_2 plane.

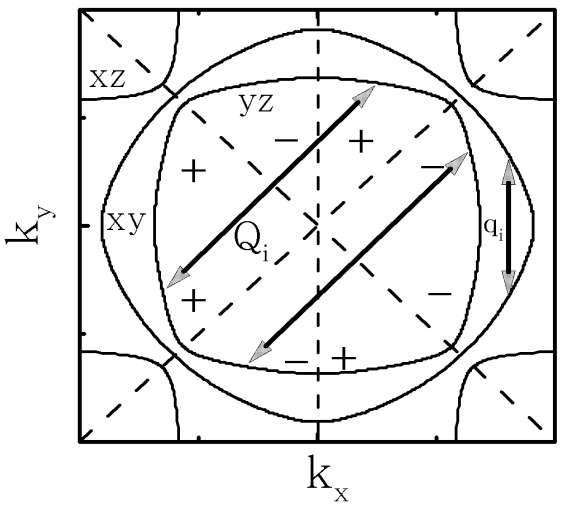

Fig. 9 Symmetry analysis of the order parameter for triplet pairing in the first BZ for $k_z = 0$ (solid curves) and $k_z = \pi/2c$ (dotted curves). α, β, and γ denote the FS of the corresponding hybridized bands. The wave vectors $\mathbf{Q}_i$ and $\mathbf{q}_i$ are the main wave vectors contributing to the susceptibility (without spin-orbit coupling). For $f_{x^2-y^2}$-wave symmetry the nodes of the real part of the order parameter are shown (dashed lines) and the regions $+(-)$ where the $f_{x^2-y^2}$-wave superconducting gap is positive (negative). Note, for the real part of a p-wave order parameter the node would occur only along $k_x = 0$.

The wave vectors $\mathbf{Q}_i$ and $\mathbf{q}_i$ refer to the peaks in $\chi(\mathbf{q},\omega)$. The areas with $\Delta_{f_{x^2-y^2}} > 0$ and $\Delta_{f_{x^2-y^2}} < 0$ are denoted by (+) and (-), respectively. Note, that the minus sign in eq. (16) is absent for triplet pairing. The summation over $\mathbf{k}'$ in the first BZ is dominated by the contributions due to $\mathbf{Q}_i$ for the α- and β-bands and the one due to $\mathbf{q}_i$ for the γ-band.

As can be seen from Fig. 9 in the case of $f_{x^2-y^2}$-wave symmetry for the $xy-$band the wave vector $\mathbf{q}_i$ bridges the same number of portions of the FS with opposite and equal sign. Therefore, for the xy-band no solution with $f_{x^2-y^2}$-wave symmetry is possible. On the other hand, for the $xz-$ and yz-band the wave vector $\mathbf{Q}_i$ bridges portions of the FS with *equal* signs of the $f_{x^2-y^2}$-superconducting order parameter. The eigenvalue of this order parameter is also enhanced due the interband nesting for xz and yz-bands. Thus, superconductivity in the xz- and yz-band in the RuO_2 plane is indeed possible with $f_{x^2-y^2}$-wave order parameter. Therefore, solving eq. (16) for the three band picture we found a competition between triplet p-wave and $f_{x^2-y^2}$-wave superconductivity in the RuO_2-plane.

We can immediately rule out singlet Cooper-pairing. In particular, assuming $d_{x^2-y^2}$-symmetry for Sr_2RuO_4 the eq. (16) yields an eigenvalue which is lower than in the case of triplet pairing. As can be seen using Fig. 9 this is plausible. Note, we get for $d_{x^2-y^2}$-wave symmetry a change of sign of the order parameter upon crossing the diagonals of the BZ. According to eq. (16) wave vectors around $\mathbf{Q}_i$ connecting areas (+) and (-) contribute constructively to the pairing. Contributions due to $\mathbf{q}_i$ and the background connecting areas with the same sign subtract from the pairing (see Fig. 9 with nodes at the diagonals). Therefore, we find that the four contributions due to $\mathbf{q}_i$ in the $xy - band$ do not allow $d_{x^2-y^2}$-wave symmetry in the $xy-$band. Despite the pair-building contribution due to $\mathbf{Q}_i$ one finds that the eigenvalue of the $d_{x^2-y^2}$-wave symmetry in the xy-band is smaller than for the $f_{x^2-y^2}$-wave symmetry. This is due to the large contribution from $\mathbf{Q}_i$ to the cross-terms for the triplet pairing which are absent for singlet pairing. For d_{xy}-symmetry where the nodes are along (π,0) and (0,π) directions we argue similarly. Thus, we exclude this symmetry.

The $f_{x^2-y^2}$-wave symmetry solution has vertical lines of nodes along the k_z-axis. In principle, this has to be observable in the strong four-fold anisotropy of the thermal conductivity $\kappa(\theta, H)$ in applied magnetic field along ab-plane. One has to admit, however, the recent measurements have shown only a weak anisotropy [27] that suggests the line nodes in Sr_2RuO_4 are not vertical.

A phenomenological mechanism to produce horizontal line nodes has been proposed by Zhitomirskiy and Rice [30]. As we have already mentioned, the magnetic fluctuations are different with respect to the various bands. The ferromagnetic fluctuations are originating from the xy-band while the incommensurate antiferromagnetic fluctuations are due to the nesting of xz and yz-bands. In this case it was proposed that in the active xy-band the superconducting gap has no nodes and can be described by the nodeless p-wave gap. Then, due to interband scattering of the Cooper-pairs the superconductivity is induced in the xz and yz-bands with the symmetry

$$\mathbf{d_2}(\mathbf{k}) \sim \left(\sin\frac{k_x a}{2}\cos\frac{k_y a}{2} + \sin\frac{k_y a}{2}\cos\frac{k_x a}{2}\right)\cos\frac{k_z c}{2}\,. \tag{23}$$

Note, this gap has the horizontal line of nodes at $k_z = \pm\pi/c$. Then even a combination of the nodeless p-wave symmetry and that with nodes will still be present, only the position of the nodes will be slightly shifted along c-axis. This behavior correctly describes the temperature dependence of the specific heat below T_c [30]. A similar model was proposed by Annett et al. [31]. In this model there are two distinct attractive pairing interactions. One, acting between nearest neighbor in-plane xy orbitals, leads to a nodeless chiral p-wave state on the γ-band. The second acts between nearest neighbors between planes, and is assumed to act primarily on the d_{xz} and d_{yz} orbitals, which have lobes perpendicular to the planes. This second interaction produces a gap with line nodes on the α and β Fermi surface sheets. This gap model was shown to be in quite good agreement with experiments on specific heat [25], penetration depth [28] and thermal conductivity [32]. Similar to the Zhitomirskiy Rice approach [30], this model is also 'orbital dependent superconductivity', but in this case there are no 'active' and 'passive' bands, since all bands have a pairing interaction and the gap is of similar magnitude on all three Fermi surface sheets.

Alternatively, interlayer coupling models have been proposed [33–35]. These also give rise to gap functions of the form of eq. (23), either on one or all of the three Fermi surface sheets. The physical mechanisms responsible for the interlayer coupling and hence the gap node are assumed to be either interlayer Coulomb interactions, or dipole-dipole interactions.

The question remains whether spin fluctuations can also explain the formation of the nodes along the c-axis in the 'passive' xz and yz-bands. In order to explain this we have first to take into account the magnetic anisotropy observed by NMR in the normal state [4]. In the following we will show that spin-orbit coupling is an important interaction in the physics of Sr_2RuO_4 and we shall argue that it leads to the formation of the horizontal line nodes in the superconducting state.

2.4 Spin-orbit coupling effects in the normal and superconducting states

So far we investigated the three-band Hubbard Hamiltonian. This model neglects spin-orbit coupling and would fail to explain the magnetic anisotropy at low temperatures observed in NMR experiments [4]. Recently it has been proposed that the spin-orbit coupling may play an important role in the superconducting state of Sr_2RuO_4. In particular, it was shown by Ng and Sigrist [36] that the spin-orbit coupling lowers the free-energy of the chiral superconducting order parameter. Another indication of the importance of a spin-orbit coupling is the recent observation of the large spin-orbit coupling in the related insulating compound Ca_2RuO_4 [37]. Therefore, we extend the theory by adding to the Hubbard Hamiltonian the spin orbit coupling:

$$H_{s-o} = \lambda \sum_i \mathbf{l}_i \cdot \mathbf{s}_i \,, \tag{24}$$

Here, the effective angular momentum $\mathbf{l}_i$ operates on the three t_{2g}-orbitals on the site i and $\mathbf{s}_i$ are the electron spins. As in an earlier approach of [36] we restrict ourselves to the three orbitals, ignoring e_{2g}-orbitals and choose the coupling constant λ such that the t_{2g}-states behave like an $l = 1$ angular momentum representation. Moreover, it is known that the quasi-two-dimensional xy-band is separated from the quasi-one-dimensional xz- and yz-bands. Then, one expects that the effect of spin-orbit coupling is relatively small for the xy-band and can be neglected in the first approximation [38]. Therefore, we consider the effect of the spin-orbit coupling on xz- and yz-bands only. Then, the kinetic part of the Hamiltonian $H_t + H_{\rm so}$ can be diagonalized and the new energy dispersions are obtained [38]. Note, we use $\lambda = 80\,$meV in accordance with earlier estimations [36, 37].

Most importantly, the spin-orbit coupling does not break the time-reversal symmetry and therefore the Kramers degeneracy between the spin up and $down$ is not removed. The resultant Fermi surface consists of three sheets as observed in experiment [15]. Then spin-orbit coupling together with the Hubbard Hamiltonian leads to a new quasiparticle which we label with pseudo-spin and pseudo-orbital indices. Note, that despite the spin-orbit coupling causing the spin and orbit quantum numbers not to be good ones we can still identify the Cooper-pairing to be triplet or singlet. This refers now then to the pseudo-spin quantum numbers. At the same time, the magnetic behavior of Sr_2RuO_4 becomes very anisotropic due to the fact that both one-particle Green's functions and Landé g-factors will be different if the magnetic field is applied along the c-axis or in the ab-RuO_2 plane. The anisotropy arises mainly from the calculations of the Landé g-factors and, in particular, their orbital parts. The factors $g_z = \tilde{l}_z + 2s_z$ and $g_+ = \tilde{l}_+ + 2s_+$ are calculated using the new quasiparticle states. The latter consist, for example, of xz- and yz-orbitals which in turn are the combinations of the initial orbital states $|2, +1>$ and $|2, -1>$ mixed due to the crystal field. Then, the matrix elements $<|l_+|>, <|l_-|>$ are zero for the xz- and yz-orbitals while the $<|l_z|>$ matrix element is not. Therefore, the longitudinal components of the spin susceptibility of the xz- and yz-band get enhanced in comparison to the transverse one. One of the interesting questions that we will analyze later is the effect of spin-orbit coupling on the antiferromagnetic and ferromagnetic fluctuations. This provides insights into a microscopic explanation of the pairing mechanism and allows us to calculate the spatial structure of the superconducting order parameter.

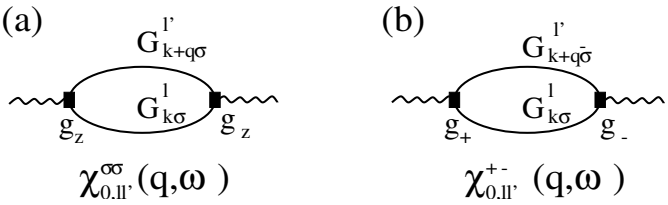

Fig. 10 Diagrammatic representation of (a) the longitudinal and (b) the transverse magnetic susceptibility. The full lines represent the electron Green's function with pseudo-spin σ and pseudo-orbital l quantum numbers. The Lande's g-factors are denoted by $g_+ = l_+ + 2s_+$ ($g_- = l_- + 2s_-$) and $g_z = l_z + 2s_z$.

For the calculation of the transverse, χ_l^{+-}, and longitudinal, χ_l^{zz}, components of the spin susceptibility of each band l we use the diagrammatic representation shown in Fig. 10. Note that because the Kramers degeneracy is not removed by spin-orbit coupling $G^l_{k,+-} = G^l_{k,zz}$. Thus, as we have already mentioned before, the anisotropy arises mainly from the calculations of the Lande's g-factors and in particular their orbital parts. The factors $g_z = \tilde{l}_z + 2s_z$ and $g_+ = \tilde{l}_+ + 2s_+$ are calculated using the new quasiparticle states. The latter consist, for example, of xz- and yz-orbitals which in turn are the combinations of the initial orbital states $|2,+1>$ and $|2,-1>$ mixed due to the crystal field. Then, the same matrix elements as above are zero for the xz- and yz-orbitals while $<|l_z|>$ matrix element is again not. Therefore, the longitudinal components of the spin susceptibility of the xz- and yz-band get enhanced in comparison to the transverse one. We obtain, for example, for the $|xz\rangle$-states for the transverse susceptibility

$$\chi^{+-}_{0,xz}(\mathbf{q},\omega) = -\frac{4}{N}\sum_{\mathbf{k}}(u_{2\mathbf{k}}u_{2\mathbf{k+q}} - v_{2\mathbf{k}}v_{2\mathbf{k+q}})^2\,\frac{f(\epsilon^+_{\mathbf{k}xz}) - f(\epsilon^-_{\mathbf{k+q}xz})}{\epsilon^+_{\mathbf{k}xz} - \epsilon^-_{\mathbf{k+q}xz} + \omega + iO^+}\,, \tag{25}$$

and for the longitudinal susceptibility

$$\begin{aligned}\chi^{zz}_{0,xz}(\mathbf{q},\omega) &= \chi^{\uparrow}_{xz}(\mathbf{q},\omega) + \chi^{\downarrow}_{xz}(\mathbf{q},\omega)\\ &= -\frac{2}{N}\sum_{\mathbf{k}}\Big[u_{2\mathbf{k}}u_{2\mathbf{k+q}} + v_{2\mathbf{k}}v_{2\mathbf{k+q}} + \sqrt{2}(u_{2\mathbf{k}}v_{2\mathbf{k+q}} + v_{2\mathbf{k}}u_{2\mathbf{k+q}})\Big]^2\\ &\quad\times\frac{f(\epsilon^+_{\mathbf{k}xz}) - f(\epsilon^+_{\mathbf{k+q}xz})}{\epsilon^+_{\mathbf{k}xz} - \epsilon^+_{\mathbf{k+q}xz} + \omega + iO^+}\,.\end{aligned} \tag{26}$$

Here, $f(x)$ is again the Fermi function and $u^2_{\mathbf{k}}$ and $v^2_{\mathbf{k}}$ are the corresponding coherence factors [38] For all other orbitals the calculations are similar and straightforward.

Then, one gets within RPA the following expressions for the transverse susceptibility

$$\chi^{+-}_{\mathrm{RPA},l}(\mathbf{q},\omega) = \frac{\chi^{+-}_{0,l}(\mathbf{q},\omega)}{1 - U\chi^{+-}_{0,l}(\mathbf{q},\omega)}\,, \tag{27}$$

and for the longitudinal susceptibility

$$\chi^{zz}_{\mathrm{RPA},l}(\mathbf{q},\omega) = \frac{\chi^{zz}_{0,l}(\mathbf{q},\omega)}{1 - U\chi^{zz}_{0,l}(\mathbf{q},\omega)}\,, \tag{28}$$

where $\chi^{zz}_{0,l} = \chi^{++}_{0,l} + \chi^{--}_{0,l}$. These susceptibilities are used in the corresponding pairing interaction for triplet pairing. In order to compare our results with NMR and INS experiments we take

$$\chi^{zz}_{\mathrm{tot}} = \sum_l \chi^{zz}_{\mathrm{RPA},l} \tag{29}$$

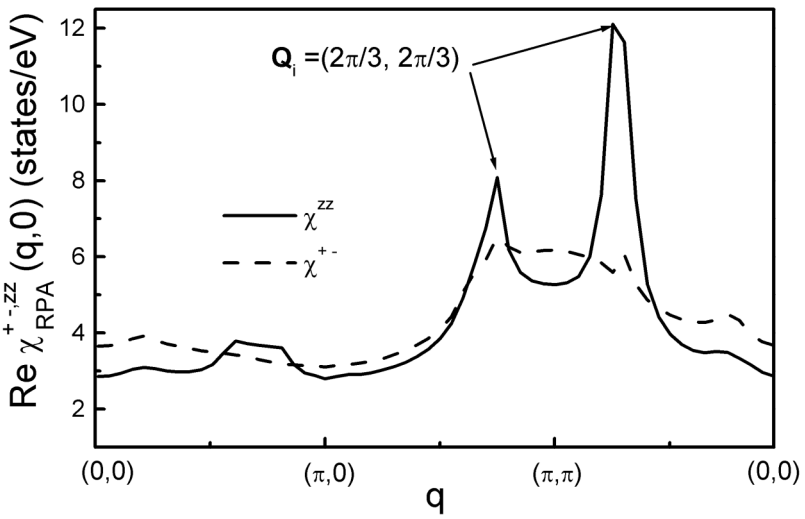

Fig. 11 Calculated real part of the longitudinal and transverse components of the total RPA spin susceptibility $\chi^{+-,zz}_{\rm RPA} = \sum_l \chi^{+-,zz}_{l,\,RPA}$ (l refers to the band indices) in the normal state of Sr_2RuO_4 along the route $(0,0) \rightarrow (\pi,0) \rightarrow (\pi,\pi) \rightarrow (0,0)$ in the first BZ. Due to spin-orbit interaction the transverse component (χ^{+-}) doe not contain incommensurate antiferromagnetic fluctuations (IAF) from xz and yz-orbitals, while in the longitudinal component (χ^{zz}) they are enhanced.

and

$$\chi^{+-}_{\rm tot} = \sum_l \chi^{+-}_{{\rm RPA},l}\,. \tag{30}$$

Using the random phase approximation(RPA) for each particular band we calculate the longitudinal and transverse components of the total susceptibility in the RuO_2-plane. Its real parts at $\omega = 0$ are shown in Fig. 11. As a result of the spin-orbit coupling the magnetic response becomes very anisotropic along the whole Brillouin Zone. Since the spin and orbital degrees of freedom are mixed now, the orbital anisotropy will be reflected in the magnetic susceptibility. As one sees in Fig. 11 the longitudinal component has a pronounced peak at $\mathbf{Q}_i$, while the transverse one does not show these features at all and is almost isotropic (it reproduces mostly the response of the xy-band). In order to understand why the longitudinal susceptibility shows mostly the nesting features of the xz- and yz-bands one has to remember that due to spin-orbit coupling the orbital component of the magnetic susceptibility cannot be neglected. Therefore, the matrix elements such as $< i|l_z|j >$ and $< i|l_{+(-)}|j >$ have to be taken into account. At the same time the xz- and yz-bands consist of the $|2,+1>$ and $|2,-1>$ orbital states. One sees that while the longitudinal component gets an extra term due to l_z, the transverse component does not, since the transitions between states $|2,+1>$ and $|2,-1>$ are not allowed. Thus, the contribution of the nesting of the xz and yz orbitals to the longitudinal component of the susceptibility is larger than to the transverse one and incommensurate antiferromagnetic fluctuations are almost absent.

In order to demonstrate the temperature dependence of the magnetic anisotropy induced by the spin-orbit coupling we display in Fig. 12 the temperature dependence of the quantity

$$\sum_{\mathbf{q}} \frac{{\rm Im}\,\chi_{\rm RPA}(\mathbf{q},\omega_{sf})}{\omega_{sf}}$$

for both components. At room temperature both longitudinal and transverse susceptibilities are almost identical, since thermal effects wash out the influence of the spin-orbit interaction. With decreasing temperature

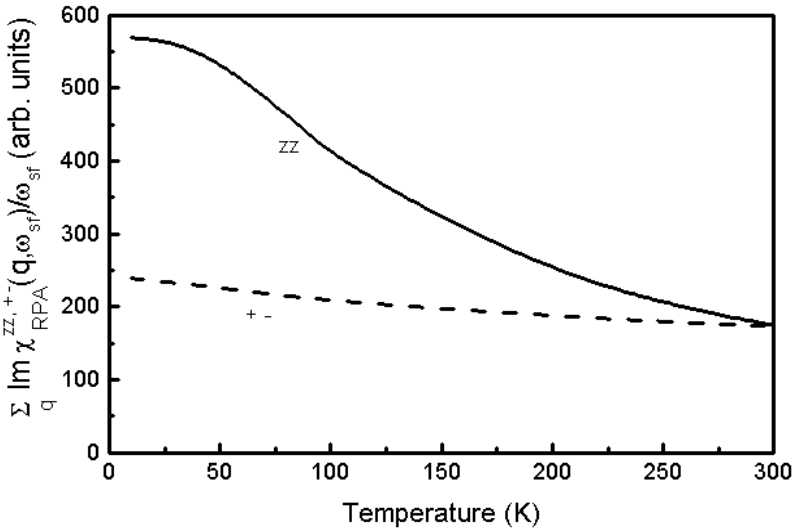

Fig. 12 Temperature dependence of the magnetic anisotropy reflected by the imaginary part of the spin susceptibility divided by ω_{sf} and summed over $\mathbf{q}$. Note, zz and $+-$ refer to the out-of-plane (solid curve) and in-plane (dashed curve) components of the RPA spin susceptibility.

the magnetic anisotropy increases and at low temperatures we find the important result that the out-of-plane component χ^{zz} is about two times larger than the in-plane one:

$$\chi^{zz} > \chi^{+-}/2\,.$$

We also note that our results are in accordance with earlier estimations made by Ng and Sigrist [39]. However, there is one important difference. In their work it was found that the IAF are slightly enhanced in the longitudinal components of the xz- and yz-bands in comparison to the transverse one. In our case we have found that the longitudinal component of the magnetic susceptibility is strongly enhanced due to orbital contributions. Moreover, we have shown by taking into account the correlation effects within RPA that the IAF are further enhanced in the z-direction.

Finally, in order to compare our results with experimental data we calculate the nuclear spin-lattice relaxation rate T_1^{-1} for the ^{17}O ion in the RuO_2-plane for different external magnetic field orientation ($i = a, b,$ and c):

$$\left[\frac{1}{T_1 T}\right]_i = \frac{2k_B\gamma_n^2}{(\gamma_e\hbar)^2}\sum_{\mathbf{q}}|A_{\mathbf{q}}^p|^2\,\frac{\chi_p''(\mathbf{q},\omega_{sf})}{\omega_{sf}}\,, \tag{31}$$

where $A_{\mathbf{q}}^p$ is the q-dependent hyperfine-coupling constant perpendicular to the i-direction.

In Fig. 13 we show the calculated temperature dependence of the spin-lattice relaxation for an external magnetic field within and perpendicular to the RuO_2-plane together with experimental data. At $T = 250$ K the spin-lattice relaxation rate is almost isotropic. Due to the anisotropy in the spin susceptibilities arising from spin-orbit coupling the relaxation rates become increasingly different for decreasing temperature. The largest anisotropy occurs close to the superconducting transition temperature in good agreement for experimental data [8].

Note, most recently similar magnetic anisotropy has been observed by means of inelastic neutron scattering [40]. However, the absolute magnitude of the anisotropy seems to be smaller than in the case of the NMR experiments [8]. The reason for this might be that in the NMR experiments the magnetic susceptibility is summed over the whole Brillouin Zone while in the INS only its part around $\mathbf{Q} = (2\pi/3, 2\pi/3)$ is probed.

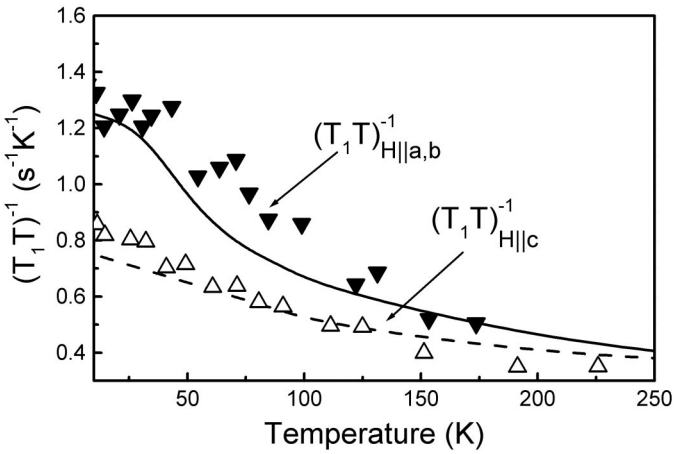

Fig. 13 Calculated normal state temperature dependence of the nuclear spin-lattice relaxation rate T_1^{-1} of ^{17}O in the RuO_2-plane for an external magnetic field applied along c-axis (dashed curve) and along the ab-plane (solid curve) using eq. (31). Triangles are experimental results taken from [8].

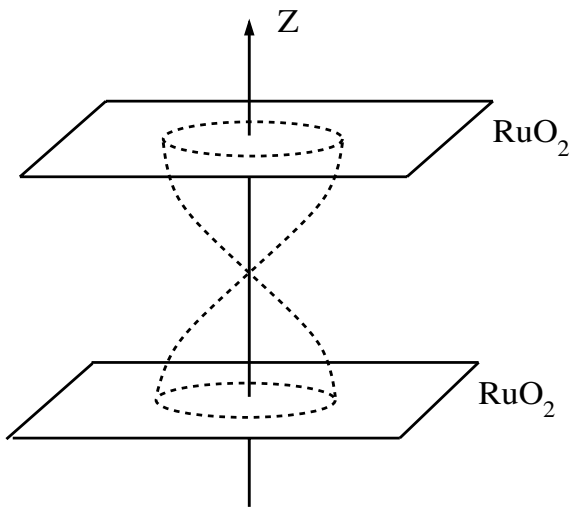

Fig. 14 Schematic representation of the possible node formation in the order parameter between the RuO_2-planes (in real coordinate representation) as resulting from the magnetic anisotropy. Here, the amplitude of the order parameter along the z-direction has been drawn in cylindrical coordinates between RuO_2-planes. This horizontal line node in the superconducting gap resulting from antiferromagnetic spin fluctuations along z-direction seems to be in agreement with thermal conductivity measurements below T_c [27].

What is the influence of spin-orbit coupling for determining the symmetry of the superconducting gap in Sr_2RuO_4? First, the spin-orbit coupling affects the spin dynamics and as we have shown induces the anisotropy in the spin subspace. In particular the two-dimensional IAF at $\mathbf{Q}_i = (2\pi/3, 2\pi/3)$ have a polarization along the z-direction. This simply means that the antiferromagnetic moments associated with these fluctuations align along the z-direction. At the same time the ferromagnetic fluctuations are in the ab-plane. This is illustrated in Fig. 14. Since the interaction in the RuO_2-plane ($k_z = 0$) is mainly ferromagnetic nodeless p-wave pairing is indeed possible and the superconducting order parameter in all three bands will not have nodes. This differs from previous results in which only the xy-band was nodeless. Therefore, we safely conclude that triplet p-wave pairing without line-nodes will be realized in the RuO_2-plane. On the other hand the state between the RuO_2-plane will be determined mainly by the IAF that are polarized along the c-direction. This implies that the magnetic interaction between the planes has to be rather antiferromagnetic than ferromagnetic. This antiferromagnetic interaction strongly suggests a line of nodes for $\Delta(\mathbf{k})$ between the neighboring RuO_2-planes. This is in agreement with the arguments presented in [30]. Then, due to the magnetic anisotropy induced by spin-orbit coupling a nodeless $p-$wave pairing is possible in the RuO_2-plane as experimentally observed [27], while a node would lie between the RuO_2-planes.

Note, the spin-orbit coupling determines also the orientation of the $\mathbf{d}$-vector of the Cooper-pairs. In a triplet superconductor, the pairing state can be represented by the three-dimensional vector $\mathbf{d}(\mathbf{k})$, whose magnitude and direction may vary over the Fermi surface in $\mathbf{k}$-space. Like in the case of superfluid ^{3}He,

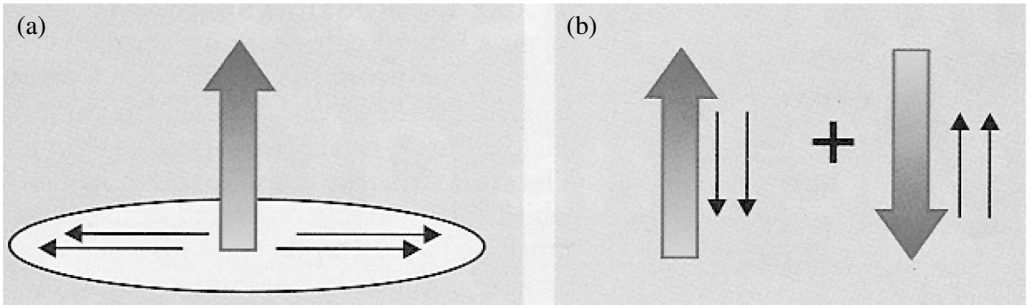

Fig. 15 Illustration of the possible superconducting states in Sr_2RuO_4 taken from [42]. (a) $\Delta(\mathbf{k}) = d_z(\sin k_x + i \sin k_y)$ and (b) $\Delta(\mathbf{k}) = d_x \sin k_x + d_y \sin k_y$ have different spin and total angular momentum. The $\Delta(\mathbf{k}) = d_z(\sin k_x + i \sin k_y)$ superconducting state has an angular momentum along c-axis (thick arrow) and the spin is lying in the RuO_2-plane.

several pairing states related to the different orientation of the total spin moment of the Cooper-pair d_z, d_y, d_z may have the same condensation energy under weak-coupling conditions. This degeneracy is related to the spin rotation symmetry being present in ^{3}He (which leads to presence of the so-called B-phase), but is lifted by the spin-orbit coupling in Sr_2RuO_4 [36]. Then, the analogy of the A-phase-like can be realized in Sr_2RuO_4 ($\mathbf{d}(\mathbf{k})_A$ = (0,0,$d_z(k_x \pm ik_y)$)) while the two-dimensional analog of the B-phase will be suppressed ($\mathbf{d}(\mathbf{k})_B = |d|(k_x, k_y, 0)$). The different orientation of the spin and orbital angular momenta of the Cooper-pair is illustrated in Fig. 15 . The important consequence of this order parameter is the uncompensated orbital angular momentum of the Cooper-pair (so-called 'chiral' state).

In analogy to ^{3}He, interesting effects can be observed by applying external magnetic field or external pressure along ab-plane to Sr_2RuO_4. For example, in ^{3}He the transition from the B to the A phase is observed under pressure while in an external magnetic field the A transition splits into A_1, A_2 phases. In Sr_2RuO_4 the situation is somewhat opposite. Superconductivity in Sr_2RuO_4 is already in the A-like phase and therefore, it would be interesting to see whether by applying pressure or magnetic field one could cause a transition into a B-like phase. Note that recently a second phase has been observed in high magnetic field applied along a-direction ($H||(100)$) with $T_c \sim 0.5\ T_{c0}$ [41]. The origin of this feature is not clear at the moment.

2.5 Comparison of superconductivity in cuprates and Sr_2RuO_4

Despite of the similar crystal structures the differences in the electronic states close to the Fermi level leads to the different electronic structure of cuprates and ruthenates. As a result the spin fluctuations are very different. In both systems the spin fluctuations are strong but while in cuprates the antiferromagnetic fluctuations at $\mathbf{Q} = (\pi, \pi)$ in Sr_2RuO_4 there is a competition between ferromagnetic and incommensurate antiferromagnetic fluctuations at $\mathbf{Q}_{\rm IAF} = (2\pi/3, 2\pi/3)$. As we have shown earlier the superconductivity in the Sr_2RuO_4 seems to be induced by mainly the ferromagnetic fluctuations and the role of IAF is in the formation of the line nodes in the passive xz and yz-bands between the RuO_2-planes.

The comparison of the superconductivity in ruthenates and cuprates was done in [43] on the basis of the $t - J - I$ model. For all cuprate compounds the degeneracy between the copper $3d$-orbitals is removed by the lattice structure. After some straightforward calculations it can be shown that the hybridized copper and oxygen orbitals separate. As shown in Fig. 16a, the state with highest (lowest) energy has mainly $d_{x^2-y^2}$-wave character in the undoped cuprates and the d^9 copper has one missing electron (i.e. a hole) and gives the Cu-ion a spin $\frac{1}{2}$. Thus, in the absence of doping, the cuprate material is well described by a model of mostly localized spin-$\frac{1}{2}$ states. The other orbitals are occupied and therefore can be neglected. However, the Coulomb repulsion between holes in the same orbital is strong and must be included. Due to the large Coulomb repulsion the $d_{x^2-y^2}$-orbitals split into two so-called lower and upper Hubbard bands

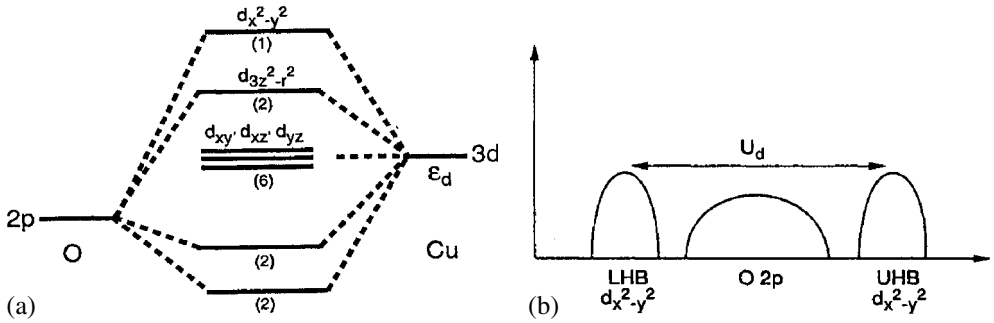

Fig. 16 Schematic electronic structure of the CuO_2-planes of cuprates reflecting bonding between a Cu^{2+} and two O^{2-} ions. (a) Initial splitting of the bands taking into account crystal field interaction only. We consider only d-electrons (holes) of Cu and p_x and p_y orbitals of the oxygen. The numbers indicate the occupations of the different levels in the undoped compound. (b) Role of the on-site Coulomb repulsion and the splitting of $3d_{x^2-y^2}$-orbital into a lower (LHB) and upper Hubbard band (UHB). U_d is the Coulomb repulsion between electrons at Copper. Due to $\delta = \epsilon_p - \epsilon_d < U_d$ the cuprates are Mott-Hubbard insulators without doping.

(LHB and UHB), respectively as shown in Fig. 16b. Then, at half-filling the system becomes an insulator. Furthermore, due to a very large U_d the splitting of $d_{x^2-y^2}$-band is so large that the oxygen p-band lies between the UHB and the LHB. The charge transfer gap in cuprates δ ($\delta = \epsilon_p - \epsilon_d$) is smaller than U_d, and so underdoped cuprates are charge-transfer insulators. When the cuprates are doped the $t - J$ model appears as an effective low-energy Hamiltonian describing the moving of a hole on the antiferromagnetic background [44].

In contrast to the cuprates, in ruthenates the Fermi level lies in the center of the d_{xy}, d_{xz}, and d_{yz} manifold of states. In the ruthenates considering the active xy-band one could also consider the moving of the electrons on the ferromagnetic background. The instability of the system can be analyzed with respect to the triplet p-wave and singlet d-wave Cooper-pairing. In a weak-coupling BCS theory it was found [43] that for p-wave pairing the van Hove singularity does not contribute to the T_c since in the effective density of states the corresponding electron velocity at the Fermi level is cancelled by the angular dependence of the p-wave superconducting gap $\sim (\sin k_x \pm i \sin k_y)$. At the same time this cancellation does not occur for $d_{x^2-y^2}$-wave Cooper pairing and thus the van Hove singularity enhances T_c.

We can also contrast the spin fluctuation pairing mechanism in the cuprates and ruthenates. In the strong-coupling Eliashberg-like theory of superconductivity in the cuprates [45] the enhancement of T_c occurs due to pronounced antiferromagnetic spin fluctuations and due to a large spectral weight of the pairing interaction at high frequencies. Therefore, by comparison of superconductivity in Sr_2RuO_4 and high-T_c cuprates one may conclude that the higher T_c in cuprates can be explained by the stronger antiferromagnetic fluctuations and the density of states effects (van Hove singularity). This, however, are only quantitative arguments since a complete theory of superconductivity in cuprates is still lacking.

3 Mott-insulator transition in $Ca_{2-x}Sr_xRuO_4$

Originally, the investigations of ruthenates were concentrated on Sr_2RuO_4 and $SrRuO_3$, since it was believed that in contrast to cuprates in ruthenates only ferromagnetic fluctuations take place. However, it was soon realized that the ruthenates reveal much more interesting behavior. In particular, the richness of the electronic, magnetic and structural phase transitions in $Ca_{2-x}Sr_xRuO_4$ has received a lot of attention recently.

In particular, in $Ca_{2-x}Sr_xRuO_4$ a transition from triplet superconductivity in Sr_2RuO_4 to an antiferromagnetic Mott-Hubbard insulator in Ca_2RuO_4 has been found [46]. For various values of x the different

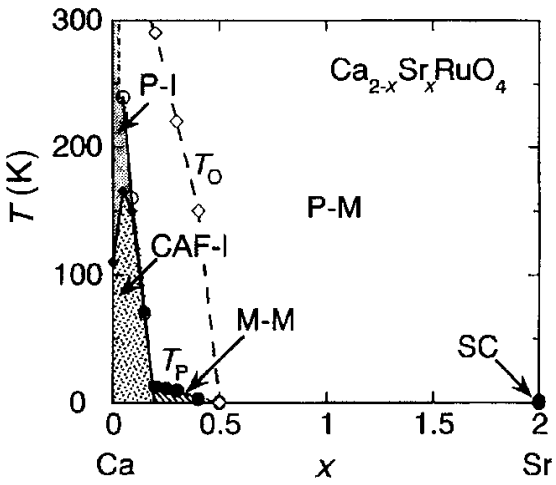

Fig. 17 Phase diagram of $Ca_{2-x}Sr_xRuO_4$. P refers to paramagnetic, CAF to canted antiferromagnetic, M to magnetic, SC to the superconducting phase, -M to the metallic phase, and -I to the insulating phase [46].

phase transitions occur as shown in Fig. 17. For example for $x < 0.2$ this material is an insulator and for the interval $0.2 < x < 0.5$ $Ca_{2-x}Sr_xRuO_4$ is a metal with short-range antiferromagnetic order. At $x \sim 0.5$ there is a crossover which is accompanied by the sharp enhancement of the ferromagnetic fluctuations in the uniform spin susceptibility. For $x \to 2$ the system becomes superconducting with triplet Cooper-pairing.

A neutron diffraction study on $Ca_{2-x}Sr_xRuO_4$ has been made recently [47], and results in the structural phase diagram of this system, shown in Fig. 18a. Here, one can see also the experimental data of the structural (T_S), magnetic (T_N) phase transition and the dashed curve refers to the temperature T_p where the magnetic susceptibility shows a maximum. As one sees for $x < 0.2$ the metal-insulator transition is accompanied by the structural transition as well where both low and high temperature phases have the symmetry $Pbca$ with only difference of the parameter c (S-short c, L-long c). In the metallic phase there are two structural phase transitions which are influencing the temperature and concentration dependencies of the magnetic susceptibility. In Fig. 18b we illustrate the evolution of the structural transitions with increasing x, starting from Sr_2RuO_4. The rotation of the RuO_6 octahedra around $c-$axis leads to a phase $I4_1/acd$. For $x = 1$ we have $\phi = 10.8$. Below $x = 0.5$ there are addition rotations around the ab-plane axis which increase the θ angle and suppression of the octahedra along the c-axis.

An attempt to explain the magnetic phase diagram of $Sr_{2-x}Ca_xRuO_4$ has been made on a basis of 'ab-initio' band structure calculations [48], as shown in Fig. 19. It was shown that the rotations of the RuO_6 octahedra around the $c-$axis stabilize the ferromagnetic state, since they are sufficient to reduce the $pd-\pi$ hybridization between the xy-orbital and the oxygen $2p$-states. Then the xy-band becomes narrower and the van Hove singularity shifts towards the Fermi level. At the same time the xz- and yz-bands are only slightly affected. On the contrary, the rotation around the ab-plane changes all three bands completely and that increases the nesting of xz- and yz-bands and may stabilize the antiferromagnetic phase [48].

In this picture it is easy to understand why the ferromagnetic fluctuation are strongly enhanced around the so-called critical doping $x \sim 0.5$. Using the LDA parameters for the tight-binding energy dispersion we calculated the Lindhard response function of the xy-band for $Ca_{0.5}Sr_{1.5}RuO_4$ and Sr_2RuO_4 as shown in Fig. 20. One could clearly see that due to vicinity to the van Hove singularity the ferromagnetic response of the $xy(\gamma)$-band is strongly enhanced, at $\mathbf{q} = 0$. Furthermore, since the α and β-bands are almost unchanged the ferromagnetic response gets much stronger than the antiferromagnetic ones indicating the dominance of the ferromagnetic fluctuations around this critical point $x \sim 0.5$. This is in good agreement with experiment [47]. However, this model cannot explain the Mott-Hubbard transition in Ca_2RuO_4 at finite temperatures, since Ca_2RuO_4 remains an insulator even above T_N. Therefore, strong electronic correlations has to be taken into account, as was proposed recently [49]. Here it was suggested that while the xz- and yz-bands are split into the lower and upper Hubbard bands, the xy-band is not split even though it is close

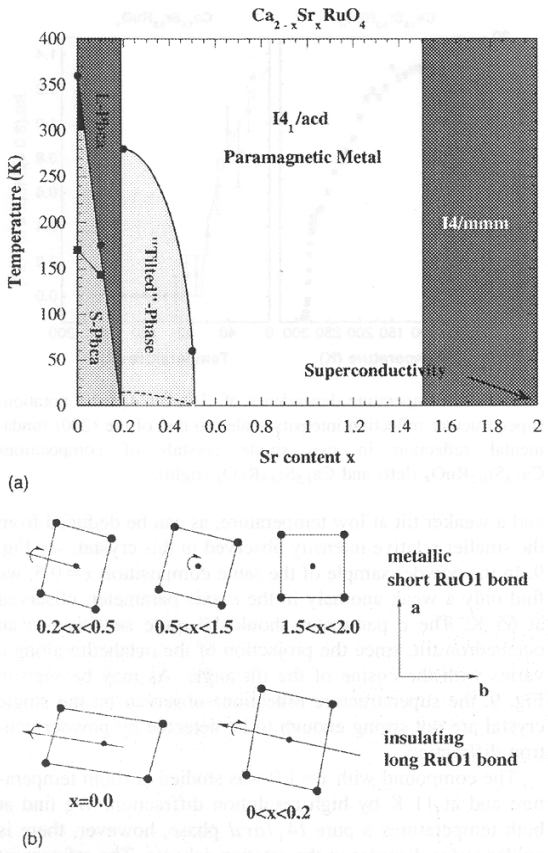

Fig. 18 Phase diagram of $Ca_{2-x}Sr_xRuO_4$ as measured by means of neutron diffraction [47] including the different structural and magnetic phases and the occurrence of the maxima in the magnetic spin susceptibility. In the lower part the tilting and rotation distortion of the octahedra are shown together with elongation of the basal planes (Ru – small points, O(1) – larger points). All phases are metallic except S–Pbca.

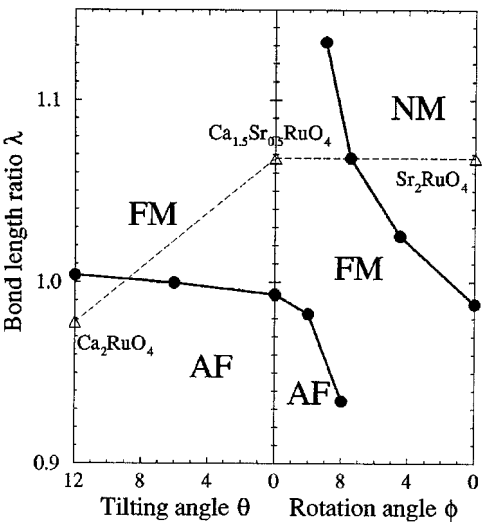

Fig. 19 The calculated magnetic phase diagram of Sr_2RuO_4 including structural distortions, taken from [48]. The solid lines are calculated phase boundaries, while the triangles linked by dashed lines correspond to the experimental data.

to the Mott-Hubbard transition. The splitting between $xz(\alpha)$- and $yz(\beta)$-bands is increased due to interband Coulomb repulsion. Indeed, in a mean-field approximation

$$U_{\alpha\beta}n_\alpha n_\beta \to U_{\alpha\beta} < n_\alpha > n_\beta + U_{\alpha\beta}n_\alpha < n_\beta > \tag{32}$$

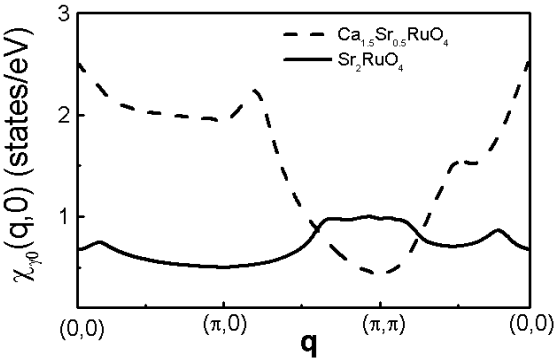

Fig. 20 The calculated real part of the Lindhard response function, $\chi_{\gamma 0}(\mathbf{q}, 0)$ along the symmetry points in the BZ in comparison for the γ-band for $Ca_{0.5}Sr_{1.5}RuO_4$ and Sr_2RuO_4. Due to vicinity to the van Hove singularity the response of the γ-band is strongly enhanced and ferromagnetic (around $\mathbf{q} = 0$). This is in good agreement with experiment [47].

the energy dispersions are renormalized

$$\epsilon_\alpha \rightarrow \tilde{\epsilon}_\alpha = \epsilon_\alpha + U_{\alpha\beta} < n_\beta >$$
$$\epsilon_\beta \rightarrow \tilde{\epsilon}_\beta = \epsilon_\beta + U_{\alpha\beta} < n_\alpha > \tag{33}$$

and the splitting of the α- and β-bands is given by

$$\Delta\epsilon = \tilde{\epsilon}_\beta - \tilde{\epsilon}_\alpha = \epsilon_\beta - \epsilon_\alpha + U_{\alpha\beta}(< n_\alpha > - < n_\beta >) \sim t_{\alpha\beta} + \tfrac{2}{3}U_{\alpha\beta}. \tag{34}$$

Here we use the data for the filling of the α and β-bands from [13]. At $U_{\alpha\beta} \approx 1\,\mathrm{eV}$ the splitting is $\Delta\epsilon \sim 0.8\,\mathrm{eV}$ which is comparable with the band width of these bands. Note in this case one will have still three Fermi surfaces (as in LDA calculations) due to the xy-band, upper Hubbard band of β-band and one hole-like Fermi surface from the α-band with filling factor $n_\gamma^h \approx 0.3$.

Due to the rotation of RuO_6-octahedra around the c-axis the width of the $xy\,(\gamma)$-band is reduced and the system approaches the critical value $U \sim U_c$. As we mentioned for the rotation of the RuO_6-octahedra around c-axis, the α and β-bands are not changing in this doping range ($0.5 < x < 2.0$). Further decreasing x and the rotation of the RuO_6-octahedra with respect to the ab-plane reduces the bandwidth of all three bands so for $x = 0$ the γ-band is split into the filled lower and empty upper Hubbard bands. A similar situation occurs for the β-band while the α-band is now just completely filled. This allows us to explain the formation of the Mott-Hubbard insulator for Ca_2RuO_4 in a way consistent with experimental data of X-ray Absorption Spectroscopy [50]. Note that while LDA+DMFT results [52] also predict correctly the formation of Mott-Hubbard antiferromagnetic insulator in Ca_2RuO_4 the resulting filling of the bands is inconsistent with the observed data [50].

In addition, a new phase transition in Ca_2RuO_4 has been found recently by applying an external hydrostatic pressure [51]. Above a very small pressure ($p_c = 0.5$ GPa) Ca_2RuO_4 shows metallic properties, and most unusually it becomes a ferromagnetic metal with a Curie temperature T_c strongly dependent on pressure. For example, just above the critical pressure $T_c = 12$ K and it reaches its maximum value of $T_c = 25$ K at 5 GPa. In general, in the Hubbard model one would expect a transition from the antiferromagnetic insulator to the paramagnetic metal. However, if one keeps in mind the multi-band nature of the metallic state, a ferromagnetic ordering is possible. Of course, a study of the mechanism of magnetic order in the multiband metallic state in Ca_2RuO_4 should be done in the future.

4 Magnetic versus non-magnetic impurities in Sr_2RuO_4

It is known that unconventional superconductors like heavy-fermion compounds or high-T_c cuprates reveal peculiar behavior if one add magnetic or non-magnetic impurities. In contrast to conventional s-wave superconductors the non-magnetic as well as the magnetic impurities act as strong pair breakers and suppress

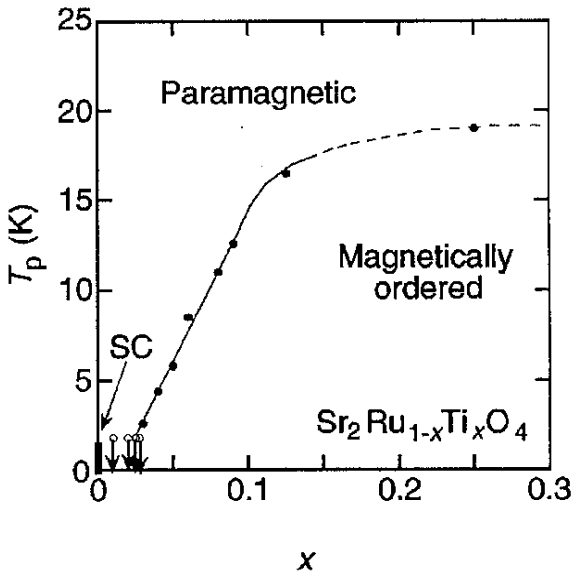

Fig. 21 Phase diagram of $Sr_2Ru_{1-x}Ti_xO_4$ [57]. The superconductivity is completely suppressed for $x > 0.02$ and it becomes magnetically ordered with $\mathbf{Q}_{ic} \sim (2\pi/3, 2\pi/3)$ indicating an importance of incommensurate antiferromagnetic fluctuations of the xz- and yz-bands for the magnetically-ordered state.

the transition temperature T_c of unconventional superconductors. The suppression of T_c reflects the sensitivity to translational symmetry breaking and is characteristic of anisotropic Cooper-pairing. In cuprates the effects induced by magnetic and non-magnetic impurities are not well understood. For example by doping the non-magnetic Zn the local magnetic moments in CuO_2-plane are induced around these impurities [53] which demonstrate Kondo-like behavior. On the contrary, the magnetic Ni impurities also show quite puzzling features which so far have not been understood [54]. The complication of the cuprates are the highly correlated electrons (holes) of the CuO_2-plane. In this respect it is of high interest to analyze the effect of impurities in Sr_2RuO_4, since it is a Fermi-liquid system in the normal state.

Early studies of the impurity effects in Sr_2RuO_4 revealed some features reflecting the unconventional nature of superconductivity. For example, the rapid suppression of T_c by native impurities and defects occurs [3] as well as the large enhancement of the residual density of states in the superconducting state seen in the specific heat [55] and NMR measurements [56].

Quite recently the first accurate study of the effects induced by the magnetic (Ir^{4+}) and non-magnetic (Ti^{4+}) impurity substitution in the RuO_2-plane has been performed [57]. Here, the observed effects are also quite peculiar. In particular, the substitution of the *non-magnetic* impurity Ti^{4+} ($3d^0$) in Sr_2RuO_4 induces a local magnetic moment with an effective moment $p_{\text{eff}} \sim 0.5\mu_B$/Ti [58]. The induced moment has Ising anisotropy with an easy axis along the c-direction. The corresponding phase diagram is shown in Fig. 21. Furthermore, magnetic ordering with glassy behavior appears for x(Ti)> 0.025 in $Sr_2Ru_{1-x}Ti_xO_4$ while retaining the metallic conduction along the in-plane direction. When x(Ti) is further increased to $x = 0.09$ the elastic neutron scattering measurements detect an incommensurate Bragg peak whose wave vector $\mathbf{Q}_{ic} \sim (2\pi/3, 2\pi/3)$ is close to the position of the inelastic neutron scattering peak in pure Sr_2RuO_4 [59]. Most interestingly, in the vicinity of a magnetic ordering a deviation from a pure Fermi-liquid behavior seen in Sr_2RuO_4 is observed by means of resistivity and transport measurements showing linear and logarithmic temperature dependencies, respectively [60]. These results indicate that the two-dimensional incommensurate antiferromagnetic spin fluctuations arising from the nesting of xz- and yz-bands become a static spin density wave state (SDW) by introducing Ti substitution. On the other hand, the system $Sr_2Ru_{1-x}Ir_xO_4$ in which the substitution is magnetic Ir^{4+} ($5d^5$ in the low spin configuration) shows a weak ferromagnetism for x(Ir) > 0.3 [61]. Thus, substitution of magnetic and non-magnetic impurities in Sr_2RuO_4 leads to a different ground states.

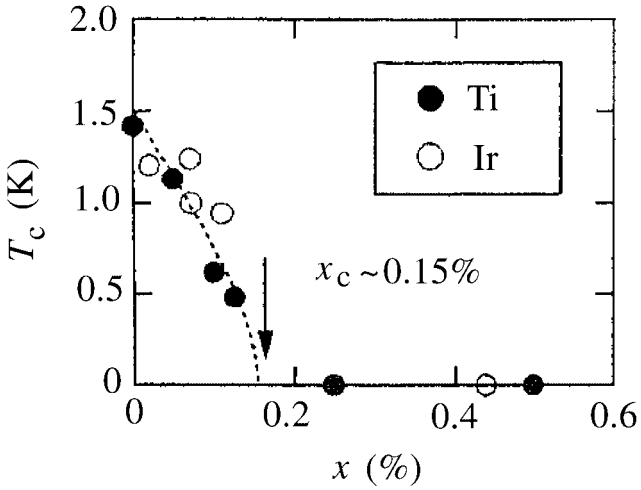

Fig. 22 Superconducting transition temperature T_c as a function of the impurity concentration x (Ti, Ir) [57]. The superconductivity is completely suppressed for $x > 0.0015$. The dashed curve shows the fit to the Abrikosov-Gor'kov pair-breaking function generalized to the case of magnetic and non-magnetic impurities in unconventional superconductors [62].

Despite of these differences both magnetic and non-magnetic impurities act similarly suppressing superconductivity in Sr_2RuO_4 for $x > 0.0015$ [57] as shown in Fig. 22. From this behavior it is clear that magnetic and non-magnetic impurities act mainly as a potential scatters for superconductivity in Sr_2RuO_4 and that the magnetic scattering does not play any role. Although this behavior could be explained in other ways, this observation is also consistent with the existence of a spin triplet state. Magnetic impurities break singlet Cooper-pairs mainly because of exchange splitting of the single particle state. The equal spin paired state would not be subject to such an effect.

More detailed theoretical investigation is still needed in order to fully understand the role played by the impurities in Sr_2RuO_4 and illuminate the role played by magnetic fluctuations in the ruthenates.

5 Conclusions

In this review we have presented some aspects of superconductivity in Sr_2RuO_4 which have not been reviewed previously in a unified way so far. Most importantly, we analyzed the role of electronic correlations and the competition between ferromagnetic and incommensurate antiferromagnetic spin fluctuations for the formation of unconventional triplet superconductivity in Sr_2RuO_4. We have found that the magnetic response is strongly anisotropic and is due to spin-orbit coupling. As we have shown it plays a crucial role in the formation of triplet p-wave superconductivity with line nodes between the RuO_2-layers. We further argue that spin-fluctuation-mediated Cooper-pairing scenario in a frame of the three-band Hubbard Hamiltonian can explain well the symmetry of the superconducting order parameter in Sr_2RuO_4. Furthermore, we point out that strong electronic correlations are responsible for the rich phase diagram of $Ca_{2-x}Sr_xRuO_4$ compound upon changing the Ca content.

We have also discussed the open issues in Sr_2RuO_4, like the influence of magnetic and non-magnetic impurities on the superconducting and normal state of Sr_2RuO_4. It is clear that the physics of triplet superconductivity in Sr_2RuO_4 is still far from being completed and remains to be analyzed more in detail.

Acknowledgements We are grateful to M. Sigrist, M. Braden, and K. H. Bennemann for stimulating discussions. The present work is supported by the INTAS Grant No. 01-654. S. G. O. is supported by the Program "Quantum Macrophysics" of the Russian Academy of Science.

References

[1] J. G. Bednorz and K. A. Müller, Z. Phys. B **64**, 189 (1986).
[2] Y. Maeno et al., Nature **372**, 532 (1994).
[3] A. P. Mackenzie et al., Phys. Rev. Lett. **80**, 161 (1998).
[4] K. Ishida et al., Phys. Rev. B **56**, 505 (1997).
[5] T. M. Rice and M. Sigrist, J. Phys., Condens. Matter **7**, L643 (1995).
[6] M. Sigrist, D. Agterberg, A. Furusaki, C. Honerkamp, K. K. Ng, T. M. Rice, and M. E. Zhitomirsky, Physica C **317–318**, 134 (1999).
[7] Y. Sidis et al., Phys. Rev. Lett. **83**, 3320 (1999).
[8] K. Ishida, H. Mukuda, Y. Kitaoka, Z. Q. Mao, H. Fukuzawa, and Y. Maeno, Phys. Rev. B **63**, 060507 (2001).
[9] T. Dahm, H. Won, and K. Maki, cond-mat/0006151 (unpublished).
[10] A. P. Mackenzie and Y. Maeno, Rev. Mod. Phys. **75**, 657 (2003).
[11] C. Noce and M. Cuoco, Phys. Rev. B **59**, 2659 (1999).
[12] T. Oguchi, Phys. Rev. B **51**, 1385 (1995).
[13] D. Singh, Phys. Rev. B **52**, 1358 (1995).
[14] A. Liebsch and A. Lichtenstein, Phys. Rev. Lett. **84**, 1591 (2000).
[15] A. P. Mackenzie et al., Phys. Rev. Lett. **76**, 3786 (1996).
Y. Yoshida et al., J. Phys. Soc. Jpn. **68**, 3041 (1999).
[16] I. I. Mazin and D. Singh, Phys. Rev. B **56**, 2556 (1997).
[17] I. I. Mazin and D. Singh, Phys. Rev. Lett. **82**, 4324 (1999).
[18] T. Imai et al., Phys. Rev. Lett. **81**, 3006 (1998).
[19] J. F. Annett, Adv. Phys. **39**, 83 (1990).
[20] J. A. Duffy et al., Phys. Rev. Lett. **85**, 5412 (2000).
[21] G. M. Luke et al., Nature **394**, 558 (1998).
[22] D. J. Scalapino, Phys. Rep. **250**, 329 (1995); N. F. Berk and J. R. Schrieffer, Phys. Rev. Lett. **17**, 433 (1966).
A. J. Layzer and D. Fay, Int. J. Magn. **1**, 135 (1971); in Proceedings of the 11th International Conference on Low Temperature Physics (LT 11) (St. Andrews Press, Edinburgh, 1968), Vol. 2, p. 760.
P. W. Anderson and W. F. Brinkmann, in: The physics of liquid and solid Helium, V. 2, edited by K. H. Bennemann and J. B. Ketterson (Wiley-Interscience, New York Chichester Brisbane Toronto, 1978).
[23] H. Kontani and K. Ueda, Phys. Rev. Lett. **80**, 5619 (1998).
[24] K. Kuroki, M. Ogata, R. Arita, and H. Aoki, Phys. Rev. B **63**, 060506(R) (2001).
[25] S. Nishizaki, Y. Maeno, and Z. Mao, J. Low Temp. Phys. **117**, 1581 (1999); J. Phys. Soc. Jpn. **69**, 572 (2000).
[26] K. Ishida et al., Phys. Rev. Lett. **84**, 5387 (2000).
[27] M. Tanatar et al., Phys. Rev. B **63**, 064505 (2001).
[28] I. Bonalde et al., Phys. Rev. Lett. **85**, 4775 (2000).
[29] I. Eremin, D. Manske, C. Joas, and K. H. Bennemann, Europhys. Lett. **57**, 447 (2002).
[30] M. E. Zhitomirsky and T. M. Rice, Phys. Rev. Lett. **87**, 057001 (2001).
[31] J. F. Annett, G. Litak, B. L. Gyorffy, and K. I. Wysokinski, Phys. Rev. B **66**, 134514 (2002).
[32] K. Izawa, H. Takahashi, H. Yamaguchi, Y. Matsuda, M. Suzuki, T. Sasaki, T. Fukase, Y. Yoshida, R. Settai, and Y. Onuki, Phys. Rev. Lett. **86**, 2653 (2001).
[33] Y. Hasegawa and M. Yakiyama, J. Phys. Soc. Jpn. **72**, 1318 (2003).
[34] Y. Yanase and M. Ogata, J. Phys. Soc. Jpn. **72**, 673 (2003).
[35] S. Koikegami, Y. Yoshida, and T. Yanagisawa, Phys. Rev. B **67**, 134517 (2003).
[36] K. K. Ng and M. Sigrist, Europhys. Lett. **49**, 473 (2000).
[37] T. Mizokawa, L. H. Tjeng, G. A. Sawatzky, G. Ghiringhelli, O. Tjernberg, N. B. Brookes, H. Fukazawa, S. Nakatsuji, and Y. Maeno, Phys. Rev. Lett. **87**, 077202 (2001).
[38] I. Eremin, D. Manske, and K. H. Bennemann, Phys. Rev. B **65**, 220502(R) (2002).
I. Eremin, D. Manske, J.-R. Tarento, and K. H. Bennemann, J. Supercond. (USA) **15**, 447 (2002).

[39] K. K. Ng and M. Sigrist, J. Phys. Soc. Jpn. **69**, 3764 (2000).
[40] M. Braden, P. Steffens, Y. Sidis, J. Kulda, P. Bourges, S. Hayden, N. Kikugawa, and Y. Maeno, cond-mat/0307662 (unpublished).
[41] K. Deguchi, M. Tanatar, Z. Mao, T. Ishiguro, and Y. Maeno, J. Phys. Soc. Jpn. **71**, 2839 (2002).
[42] Y. Maeno, T. M. Rice, and M. Sigrist, Phys. Today **1**, 42 (2001).
[43] E. V. Kuz'min, S. G. Ovchinnikov, and I. O. Baklanov, Phys. Rev. B **61**, 15392 (2000).
[44] F. C. Zhang and T. M. Rice, Phys. Rev. B **37**, (1987).
[45] K. H. Bennemann and J. Ketterson (eds.), Physics of Superconductors (Springer-Verlag, Berlin, 2003).
[46] S. Nakatsuji and Y. Maeno, Phys. Rev. Lett. **84**, 2666 (2000); Phys. Rev. B **62**, 6458 (2000).
[47] O. Friedt et al., Phys. Rev. B **63**, 174432 (2001).
[48] Z. Fang and K. Terakura, Phys. Rev. B **64**, 020509 (2001).
[49] S. G. Ovchinnikov, in: Ruthenate and Rutheno-Cuprate Materials, Lecture Notes in Physics (Springer, Berlin, 2002).
[50] T. Mizokawa et al., Phys. Rev. Lett. **87**, 077201 (2001).
[51] F. Nakamura, T. Goko, M. Ito, T. Fujita, S. Nakatsuji, H. Fukazawa, Y. Maeno, P. Alireza, D. Forsythe, and S. R. Julian, Phys. Rev. B **65**, 220402(R) (2002).
[52] V. I. Anisimov, I. A. Nekrasov, D. E. Kondakov, T. M. Rice, and M. Sigrist, Eur. Phys. Journal B **25**, 191 (2002).
[53] A. V. Mahajan et al., Phys. Rev. Lett. **72**, 3100 (1994).
[54] A. Polkovnikov, S. Sachdev, and M. Vojta, Phys. Rev. Lett. **86**, 296 (2001).
[55] S. Nishizaki, Y. Maeno, and Z. Q. Mao, J. Low Temp. Phys. **117**, 1581 (1999).
[56] K. Ishida, H. Mukuda, Y. Kitaoka, Z. Q. Mao, H. Fukazawa, and Y. Maeno, Phys. Rev. Lett. **84**, 5387 (2000).
[57] N. Kikigawa, A. P. Mackenzie, and Y. Maeno, J. Phys. Soc. Jpn. **72**, 237 (2003).
[58] M. Minakata and Y. Maeno, Phys. Rev. B **63**, 180504(R) (2001).
[59] M. Braden et al., Phys. Rev. Lett. **88**, 197002 (2002).
[60] N. Kikigawa and Y. Maeno, Phys. Rev. Lett. **89**, 117001 (2002).
[61] R. J. Cava, B. Batlogg, K. Kiyono, and H. Takagi, Phys. Rev. B **49** 11890 (1994).
[62] R. J. Radtke, K. Levin, H.-B. Schüttler, and M. Norman, Phys. Rev. B **48**, 653 (1993).